Check for updates

Received: 13 April 2023 | Revised: 11 November 2023 | Accepted: 17 December 2023

DOI: 10.1002/cne.25589

RESEARCH ARTICLE

JCN RESEARCH IN SYSTEMS NEUROSCIENCE THE JOURNAL OF COMPARATIVE NEUROLOGY WILEY

Comparative analyses of the Smith–Magenis syndrome protein RAI1 in mice and common marmoset monkeys

Ya-Ting Chang[1,2] | Yu-Ju Lee[1,2] | Minza Haque[1,2] | Hao-Cheng Chang[1,2] | Sehrish Javed[1,2] | Yu Cheng Lin[1,2] | Yoobin Cho[1,2] | Joseph Abramovitz[1,2] | Gabriella Chin[1,2] | Asma Khamis[1,2] | Reesha Raja[1,2] | Keith K. Murai[1,2] | Wei-Hsiang Huang[1,2]

[1]Department of Neurology and Neurosurgery, Centre for Research in Neuroscience, McGill University, Montréal, Québec, Canada

[2]Brain Repair and Integrative Neuroscience Program, The Research Institute of the McGill University Health Centre, Montréal, Québec, Canada

Correspondence
Wei-Hsiang Huang, Department of Neurology and Neurosurgery, Centre for Research in Neuroscience, McGill University, QC H3G 1A3, Canada. Email: wei-hsiang.huang@mcgill.ca

Funding information
Azrieli Centre for Autism Research; Smith-Magenis syndrome Research Foundation

Abstract

Retinoic acid-induced 1 (*RAI1*) encodes a transcriptional regulator critical for brain development and function. *RAI1* haploinsufficiency in humans causes a syndromic autism spectrum disorder known as Smith–Magenis syndrome (SMS). The neuroanatomical distribution of RAI1 has not been quantitatively analyzed during the development of the prefrontal cortex, a brain region critical for cognitive function and social behaviors and commonly implicated in autism spectrum disorders, including SMS. Here, we performed comparative analyses to uncover the evolutionarily convergent and divergent expression profiles of RAI1 in major cell types during prefrontal cortex maturation in common marmoset monkeys (*Callithrix jacchus*) and mice (*Mus musculus*). We found that while RAI1 in both species is enriched in neurons, the percentage of excitatory neurons that express RAI1 is higher in newborn mice than in newborn marmosets. By contrast, RAI1 shows similar neural distribution in adult marmosets and adult mice. In marmosets, RAI1 is expressed in several primate-specific cell types, including intralaminar astrocytes and MEIS2-expressing prefrontal GABAergic neurons. At the molecular level, we discovered that RAI1 forms a protein complex with transcription factor 20 (TCF20), PHD finger protein 14 (PHF14), and high mobility group 20A (HMG20A) in the marmoset brain. *In vitro* assays in human cells revealed that TCF20 regulates RAI1 protein abundance. This work demonstrates that RAI1 expression and protein interactions are largely conserved but with some unique expression in primate-specific cells. The results also suggest that altered RAI1

Abbreviations: ANOVA, analysis of variance; Bdnf, brain-derived neurotrophic factor; CAMKII, Ca^{2+}/calmodulin-dependent protein kinase II; Cas9, CRISPR-associated protein 9; CRISPR, clustered regularly interspaced short palindromic repeats; CTX, cortex, DAPI, 4′,6-diamidino-2-phenylindole; Gad67, glutamate decarboxylase 67; GAPDH, glyceraldehyde 3-phosphate dehydrogenase; GFAP, glial fibrillary acidic protein; HMG20A, high mobility group 20a; HRP, horseradish peroxidase; MECP2, methyl CpG binding protein 2; MEIS2, meis homeobox 2; NEUROD2, neuronal differentiation 2; NR1, N-Methyl-D-aspartic acid receptor 1; PBS, phosphate-buffered saline; PHF14, PHD finger protein 14; p-HH3, phosphor-Histone H3; PTLS, Potocki–Lupski syndrome; RAI1, retinoic acid induced 1; RARα, retinoic acid receptor alpha; SMS, Smith–Magenis syndrome; TBS, Tris-buffered saline; TCF20, transcription factor 20; VZ, ventricular zone.

This is an open access article under the terms of the Creative Commons Attribution-NonCommercial-NoDerivs License, which permits use and distribution in any medium, provided the original work is properly cited, the use is non-commercial and no modifications or adaptations are made.
© 2024 The Authors. The *Journal of Comparative Neurology* published by Wiley Periodicals LLC.

abundance could contribute to disease features in disorders caused by *TCF20* dosage imbalance.

KEYWORDS
Callithrix jacchus, common marmoset, prefrontal cortex, RAI1, Smith–Magenis syndrome

1 | INTRODUCTION

Human brain development and function are highly sensitive to the expression levels of selective dosage-sensitive genes (Javed, Selliah, Lee, & Huang, 2020). A prime example of this sensitivity is the genetic haploinsufficiency of retinoic acid-induced 1 (*RAI1*) or a 17p11.2 microdeletion containing *RAI1*, which causes Smith–Magenis syndrome (SMS), a neurodevelopmental disorder associated with infantile hypotonia, obesity, epileptiform electroencephalographic abnormalities, and behavioral phenotypes characteristic of autism spectrum disorders (Slageret al., 2003). SMS patients carrying *RAI1* point mutations or a 17p11.2 deletion share overlapping neurological and psychiatric symptoms, suggesting that *RAI1* is the dose-sensitive gene that determines the characteristic disease features of SMS. Duplication of the SMS-causative 17p11.2 region results in *RAI1* overexpression and Potocki–Lupski syndrome (PTLS) (Potocki et al., 2000), which is a distinct neurodevelopmental disorder. In addition to its involvement in syndromic autism, *RAI1* is among the top 130 genes strongly associated with idiopathic autism (Trost et al., 2022). This clinical evidence suggests that proper *RAI1* levels are essential for brain development and function.

Mouse *Rai1* was first identified as a retinoic acid-inducible gene in the P19 carcinoma cell line (Imai et al., 1995). The retinoic acid-responsive transcriptional network is critical for regulating gene expression, dendritic spine formation, and circuit connectivity in the brain, particularly in the prefrontal cortex (Shibata et al., 2021). In the human brain, RAI1 is enriched in the neurons residing in brain regions important for cognitive and motor skills, including the cortex, hippocampus, and cerebellum (Fragoso et al., 2015). Human and mouse RAI1 proteins share 82% sequence identity (Huang et al., 2016), and our current knowledge of RAI1 function relies heavily on studying genetic mouse models. Deleting *Rai1* from the mouse brain recapitulates SMS-like features, including hyperphagia, repetitive rearing, and abnormal social dominance behavior (Bi et al., 2005; Bi et al., 2007; Huang et al., 2018; Rao et al., 2017). In the mouse brain, RAI1 protein expression is enriched in neurons but not astrocytes (Huang et al., 2016). The importance of RAI1 in neurons is further supported by our work showing that deleting the *Rai1* gene in glutamatergic or GABAergic neurons (but not astrocytes) in mice recapitulates several disease-related behavioral phenotypes resembling those observed in SMS patients (Y. T. Chang et al., 2022; Huang et al., 2016; Javed et al., 2023). We also showed that RAI1 function remains critical in the adult brain, as evidenced by postnatal genetic *Rai1* ablation in mice, resulting in energy homeostasis defects and reduced expression of brain-derived neurotrophic factor (*Bdnf*) mRNA (Javed etal., 2021). Importantly, loss of RAI1 does not damage brain function irreparably. Using the method of clustered regularly interspaced short palindromic repeat (CRISPR) activation-mediated gene therapy, we increased *Rai1* mRNA levels, partially rescued *Bdnf* expression, and reversed selective disease-related behavioral phenotypes in SMS mice (H. C. Chang et al., 2022). These data suggest that RAI1 regulates neural function in the developing and adult brains in a cell-type-specific manner. Therefore, it is essential to carefully examine the cellular expression profile of RAI1 during neocortical development and in adulthood. We focused on the prefrontal cortex because SMS mice show decreased dendritic spine density in the medial prefrontal region (Huang et al., 2018). In humans, the prefrontal cortex shows the highest retinoic acid concentration among different cortical regions (Shibata et al., 2021). This suggests that retinoic acid-responsive genes, such as *RAI1*, play potentially important roles in the prefrontal cortex.

A fundamental challenge in understanding human diseases using mouse models lies in the paucity of face validity. For instance, the neurobehavioral phenotypes of *Rai1* heterozygous mice are relatively mild (Bi et al., 2005; Bi et al., 2007; Huang et al., 2018). This contrasts with SMS patients' severe cognitive, circadian, physiological, psychiatric, and behavioral deficits (Smith et al., 1998). These discrepancies likely stem from the considerable evolutionary distance between rodents and primates, which results in divergent genetic and brain structures (Geschwind & Rakic, 2013). To extend our knowledge of RAI1 function to nonhuman primates, we characterized the spatiotemporal distribution and molecular interactions of RAI1 in the common marmoset (*Callithrix jacchus*), an emerging nonhuman primate model (Izpisua Belmonte et al., 2015; Miller et al., 2016). By performing comparative immunocytochemistry analyses using marmosets and mice, we identified unique and shared patterns of RAI1 expression between these species. Biochemistry experiments using marmoset and mouse brains revealed that RAI1 forms a protein complex in both species with a paralogous protein TCF20 and two other chromatin-binding proteins, PHF14 and HMG20A. Using human cells, we found that TCF20 regulates the stability of RAI1. Our work reveals the developmental and adult expression profile of RAI1 in marmoset brains and improves our understanding of the cellular basis of SMS.

2 | METHODS

2.1 | Ethics statement

House mice (*Mus musculus*) and common marmosets (*C. jacchus*) were housed and cared for following standard operating procedures at the Research Institute of the McGill University Health Centre. All procedures were performed in accordance with the guidelines of the

10969861, 2024, 1, Downloaded from https://onlinelibrary.wiley.com/doi/10.1002/cne.25589 by Cochrane Canada Provision, Wiley Online Library on [27/01/2024]. See the Terms and Conditions (https://onlinelibrary.wiley.com/terms-and-conditions) on Wiley Online Library for rules of use; OA articles are governed by the applicable Creative Commons License

Canadian Council on Animal Care and the Montreal General Hospital Facility Animal Care Committee, with appropriate approved protocols for animal use. Four male and three female marmosets were used in this study (imaging analyses and biochemistry): (1) newborns: three males and two females; (2) adults: one male and one female. For mouse imaging analyses, 17 mice were used: (3) newborns: $n = 7$; (4) adults: three males and seven females. For biochemistry, more than 10 newborn mice of unknown sexes were used, and for adult mice, both sexes were used ($n > 3$/sex). The marmosets were continuously housed with family members and allowed full contact. The mice were housed in groups on a 12-h light/12-h dark cycle, with ad libitum access to food and water.

2.2 | Genome editing using the CRISPR/CRISPR-associated protein 9 system

We took a dual sgRNA approach to delete *TCF20* and *RAI1* from human HEK293A cells. A pair of gRNAs ("CAAACATGAGTGCAGCAAGG" and "AGGGCCCACAGAGGTCCCCA") were used to delete human *TCF20*. *RAI1* knockout clones were generated using two independent guide pairs as described previously (H. C. Chang et al., 2022). Guide-pair sequences were cloned into a pCLIP dual vector and cotransfected with a Lenti-Cas9-Blast vector into HEK293A cells, followed by puromycin selection (1 μg/mL) for 3 days. Polyclonal populations were pelleted to conduct a first-stage PCR test for the presence of the KO band in the heterogeneous mixture. After confirming that deletions could occur, single-cell sorting was performed, and monoclonal populations were screened for deletions. Four *RAI1* knockout clones and two *TCF20* knockout clones were selected for downstream analyses.

2.3 | Brain tissue preparation and immunocytochemistry

Marmoset brains were cryoprotected in 30% sucrose in phosphate-buffered saline (PBS) solution for 3 days before being embedded in Tissue Tek O.C.T. Compound (Sakura Finetek), frozen, and sectioned coronally (50 μm) with a cryostat. Free-floating sections were collected into a cryoprotectant solution containing sodium azide (0.3% w/v), ethylene glycol (30%), and glycerol (20%) in 0.05 M phosphate buffer (pH = 7.4) until processed for immunolabeling. Marmoset brain slices were UV bleached for at least 17 h, then treated with 0.3% Triton X-100/PBS solution for 30 min, blocked in 5% BSA and 2% normal donkey serum/0.3% Triton X-100/PBS (blocking solution) for 2 h at room temperature, and incubated overnight in primary antibodies for three nights at the indicated dilutions (Table 1) in blocking solution at 4°C. Marmoset brain slices were then rinsed three times for 10 min in PBST and then incubated with fluorescent tagged-secondary antibodies in a blocking solution for 2 h at room temperature. Slices were rinsed three times in PBS and mounted using 4′,6-diamidino-2-phenylindole (DAPI) Fluoromount-G mounting Medium (SouthernBiotech). Mouse brain processing and immunostaining were performed as described previously (Huang, 2022; Huang et al., 2012). To simultaneously detect RAI1 and TCF20 to determine the extent of colocalization, anti-RAI1 and anti-TCF20 antibodies (both derived from rabbits) were pre-conjugated with fluorophores using APEX Antibody Labeling Alexa 555 and Alexa 647 kits according to manufacturer's instructions (Thermo-Fisher).

2.4 | Antibody characterization

The specificity of the in-house anti-RAI1 antibody was previously validated using western blots and immunostaining of *Rai1* knockout mice (Huang et al., 2016). The anti-TCF20 antibodies were characterized in this project using western blots with CRISPR-mediated *TCF20*-knockout cells. The list of primary antibodies and dilutions used is provided in Table 1.

Ca^{2+}/calmodulin-dependent protein kinase II (CaMKII) antibody (Abcam, ab22609) was characterized by the manufacturer using western blot analysis showing an expected major band of approximately 50 kDa using human, rat, and mouse brain tissues. This antibody has been reported to recognize both phosphorylated and nonphosphorylated CamKIIα (Jung et al., 2008). In our hands, the antibody labels cells that are consistent with cortical excitatory neurons in terms of their distributions in mouse and marmoset brains.

CD31/PECAM-1 antibody (R&D systems, AF3628) was characterized by the manufacturer using direct ELISA, flow cytometry, and western blotting assays (130 kDa). Immunofluorescent analysis was performed by the manufacturer using mouse embryo, rat heart, and a bEnd.3 mouse cell line, which revealed specific immunoreactivity consistent with endothelial cells.

FLAG antibody (Sigma, F1804) was characterized by the manufacturer in transiently transfected kidney epithelial cells using immunofluorescence. We previously characterized this antibody using western blotting analysis in FLAG-tagged *Rai1* mice and found a major band of approximately 250 kDa absent in wild-type mice that do not express FLAG-tagged Rai1 (Huang et al., 2016).

Glutamate decarboxylase 67 (GAD67) antibody (Millipore, MAB5406) was characterized by immunoblotting showing a single band at 67 kDa in rat cortical homogenates (Fong et al., 2005). According to the manufacturer, this antibody has no apparent cross-reactivity with GAD65 using western blotting.

Consistent with our experience, glyceraldehyde 3-phosphate dehydrogenase (GAPDH) antibody (ProteinTech, 60004-1-Ig) was characterized by the manufacturer using western blotting experiments showing a single band at 36 KDa in various samples, including HEK293 cells and mouse brain tissues.

Glial fibrillary acidic protein (GFAP) antibody (Abcam, ab4674) was characterized by the manufacturer using flow cytometry of human brain cells and showing a single band of approximately 50 kDa in western blotting experiments using rat whole brain lysates. In our hands, this antibody specifically labels cells that coexpress S100β (an astrocytic marker) but not NEUN (a neuronal marker) in the upper cortical layers, with characteristic astrocytic morphologies in the mouse and marmoset brains. GFAP also serves as a marker for radial glial cells

10969861, 2024, 1, Downloaded from https://onlinelibrary.wiley.com/doi/10.1002/cne.25589 by Cochrane Canada Provision, Wiley Online Library on [27/01/2024]. See the Terms and Conditions (https://onlinelibrary.wiley.com/terms-and-conditions) on Wiley Online Library for rules of use; OA articles are governed by the applicable Creative Commons License

TABLE 1 Primary antibodies used in this study.

Antibody	Antigen	Host and type	Dilution	Source, #cat, RRID
CaMKII	Full-length CamKII, clone 6G9	Mouse monoclonal IgG	1:200	Abcam ab22609 AB_447192
CD31	CD31/PECAM-1 (immunogen mouse Glu18-Lys590)	Goat polyclonal IgG	1:20 (marmoset)1:50 (mouse)	R&D systems AF3628AB_2161028
FLAG	DYKDDDDK, clone M2	Mouse monoclonal IgG	1:1000 (WB)	Sigma F1804 AB_262044
GAD67	Recombinant GAD67 protein, clone 1G10.2	Mouse monoclonal IgG	1:500	Millipore MAB5406 AB_2278725
GAPDH	GAPDH fusion protein Ag0766, clone 1E6D9	Mouse monoclonal IgG	1:1000 (WB)	ProteinTech 60004-1-Ig AB_2107436
GFAP	Recombinant full-length human GFAP	Chicken polyclonal IgY	1:1000	Abcam ab4674 AB_304558
HMG20A	Human HMG20A amino acids 1-347	Rabbit polyclonal IgG	1:1000 (WB)	Thermo-Fisher 12085-2-AP AB_2117587
MEIS2	Human MEIS2 aa1-381, clone 1H4	Mouse monoclonal IgG	1:200	Abnova H00004212-M01 AB_425545
NEUN	Purified cell nuclei from mouse brain, clone A60	Mouse monoclonal IgG	1:500	Millipore MAB377 AB_2298772
NEUROD2	Human NeuroD2 amino acids 23-37	Goat polyclonal IgG	1:500	St John's Lab STJ72554 AB_2927398
NR1	Fusion protein containing sequence from the intracellular loop between transmembrane regions III and IV of NR1, clone 54.1	Mouse monoclonal IgG	1:100	Thermo-Fisher 32-0500 AB_2533060
PHF14	Human PHF14, 16 amino acids from the N-terminal half	Rabbit polyclonal IgG	1:1000 (WB)	Millipore ABE1359-25UL AB_2924888
Phospho-Histone H3	Phospho-Histone H3 (Ser10), clone 6G3	Mouse monoclonal IgG	1:100	Cell Signaling Technology 9706 AB_331748
RAI1	Mouse Rai1 amino acids 1738-1756	Rabbit polyclonal IgG	1:200 (IF)	In-houseAB_2921229
RAI1	Human RAI1 amino acids 1-100	Rabbit polyclonal IgG	1:1000 (WB)	AbcamAB_1925378
RARα	Recombinant Human RARα, clone 9α–9A6	Mouse monoclonal IgG	1:500	Millipore 04-1545 AB_10615821
REELIN	Mouse Reelin amino acids 150-500, clone G10	Mouse monoclonal IgG	1:500	Abcam ab78540 AB_1603148
S100β	Bovine brain S-100β, clone SH-B1	Mouse monoclonal IgG	1:500	Sigma S2532 AB_477499
SOX2	SRY (sex determining region Y)-box 2	Rabbit polyclonal IgG	1:100	Thermo-Fisher PA1-094AB_2539862
TBR1	T-box braintranscription factor 1	Chicken polyclonal antibodies	1:100	Millipore AB2261AB_10615497
TCF20	Human TCF20 amino acids 1909-1958	Rabbit polyclonal IgG	1:100 (IF)	Millipore SAB2106444 AB_2921230
GFAP	Recombinant Protein corresponding to aa1 to 432 from human GFAP	Polyclonalguinea pig antiserum	1:1000	Synaptic Systems 173004

residing near the cortical ventricles, and we found coexpression of GFAP with a proliferating cellular marker p-HH3.

High mobility group 20a (HMG20A) antibody (Thermo-Fisher, 12085-2-AP) was characterized by the manufacturer using western blotting analysis in Jurkat cells, showing an expected major band of approximately 45 kDa. Immunofluorescent analysis performed by the manufacturer also revealed nuclear immunoreactivity in HepG2 cells, consistent with their previously known role in transcriptional regulation (Gomez-Marin et al., 2022). In our hands, this antibody detected a previously known interaction between HMG20A

10969861, 2024, 1, Downloaded from https://onlinelibrary.wiley.com/doi/10.1002/cne.25589 by Cochrane Canada Provision, Wiley Online Library on [27/01/2024]. See the Terms and Conditions (https://onlinelibrary.wiley.com/terms-and-conditions) on Wiley Online Library for rules of use; OA articles are governed by the applicable Creative Commons License

and TCF20 in mice using an immunoprecipitation assay (Zhou et al., 2022).

Meis homeobox 2 (MEIS2) antibody (Abnova, H00004212-M01) was characterized by the manufacturer using western blotting analysis in HeLa cells, showing an expected major band of approximately 50 kDa. The manufacturer also reported that immunoreactivity was absent in 293T cells without MEIS2 overexpression. In our hands, these antibody-labeled cells reside in layer II of the newborn marmoset prefrontal cortex, consistent with reported single-cell RNA-sequencing results using primate brains (Schmitz et al., 2022).

NEUN antibody (Millipore, MAB377) was validated as neuron-specific using immunohistochemistry and immunoblotting analyses (Mullen et al., 1992). In our hands, these antibody-labeled cells are consistent with neurons but not cells expressing the glial marker GFAP in mouse and marmoset brains.

Neuronal differentiation 2 (NEUROD2) antibody (St Johns Laboratory, STJ72554) showed a cellular distribution in the nucleus in our hands, consistent with the known distribution of basic helix-loop-helix transcription factors. Widespread expression was detected in the cortices of newborn mice and marmosets, consistent with the known distribution of NEUROD2 (Ince-Dunn et al., 2006).

N-Methyl-D-aspartic acid Receptor 1 (NR1) antibody (Thermo-Fisher, 32–0500) was characterized by the manufacturer using western blotting analysis in rat brain extract, showing an expected major band of approximately 103 kDa. The manufacturer also reported the loss of immunoreactivity in mouse liver protein extract, consistent with known differential expression patterns in the brain and liver. This antibody also showed the expected cellular distribution in mouse primary neurons overexpressing NR1 (She et al., 2012).

PHD finger protein 14 (PHF14) antibody (Millipore, ABE1359-25UL) was characterized by the manufacturer using western blotting analysis in HEK293 cells, showing an expected major band of slightly below 100 kDa. Immunocytochemistry analysis performed by the manufacturer also revealed nuclear immunoreactivity in HeLa cells, consistent with the known role of PHF14 in gene regulation (Kitagawa et al., 2012). In our hands, this antibody detected a previously known interaction between PHF14 and TCF20 in mice using an immunoprecipitation assay (Zhou et al., 2022).

Phospho-Histone H3 (Ser10) (p-HH3) antibody (Cell Signaling Technology 9706) was characterized by the manufacturer using western blotting analysis in NIH/3T3 cells (untreated or treated with serum plus Calyculin A [to induce phosphorylation of H3]). Immunocytochemistry analysis performed by the manufacturer detected immunoreactivity in NIH/3T3 cells and the subventricular zone region in mice, consistent with an identity proliferating cell. In our hands, this antibody shows immunoreactivity near the ventricles of marmoset and mouse cortices.

Retinoic acid receptor alpha (RARα) antibody (Millipore, 04–1545) was characterized by the manufacturer using western blotting analysis in HL60 cells, showing an expected major band of approximately 58 kDa. Immunofluorescent analysis performed by the manufacturer also revealed nuclear immunoreactivity in HeLa cells, consistent with the previously known role of RARα in transcriptional regulation (Laursen & Gudas, 2018). In our hands, this antibody labeled RAI1$^+$ cells in the marmoset brain, consistent with the known coexpression of RAI1 and RARα in the human brain (Fragoso et al., 2015).

RAI1 antibody (Abcam, ab86599) was characterized by the manufacturer using immunocytochemistry using human ovarian carcinoma tissues and found a strong nuclear and weaker cytoplasmic signal. Western blotting analysis from HeLa cells found a strong band at 280 KDa but also some weaker bands at 230 KDa. We used this antibody for western blotting throughout this manuscript.

REELIN antibody (Abcam, ab78540) was characterized by the manufacturer using western blotting analysis in rat brain extract, showing a strong band at 388 kDa. No immunostaining was observed in *Reeler* mice lacking REELIN expression (Zhao et al., 2006). In our hands, this antibody labeled layer I cells on the surface of the newborn marmoset brain, consistent with the known distribution of REELIN$^+$ cells in the superficial layer I of the mouse cortex (Lee et al., 2014).

S100β antibody (Sigma, S2532) specifically reacts with the β-subunit of S100 but not other members of the EF-hand family proteins (Namba et al., 2005). Immunoblots with this antibody showed an expected single band of approximately 10 KDa (Tanga et al., 2006). In our hands, this antibody specifically labeled cells coexpressing GFAP (an astrocytic marker) but not NEUN (a neuronal marker), with characteristic astrocytic morphologies in mouse and marmoset brains.

SOX2 antibody (Thermo-Fisher, PA1-094) was characterized by the manufacturer using western blotting analysis using HeLa, NCCIT, NTERA-2, and C6 cells, showing a strong band at 34–40 kDa. Immunofluorescent analysis performed by the manufacturer also revealed nuclear immunoreactivity in human-induced pluripotent stem cells and NTERA-2 cells. In our hands, this antibody labeled cells near the ventricular zones with characteristics of neural progenitor cells.

TBR1 antibody (Millipore-Sigma, AB2261) was characterized by the manufacturer using immunofluorescent analyses using the mouse frontal cortex, showing a strong nuclear pattern with moderate cytoplasmic staining. Western blotting analysis was also performed using human fetal brain tissue lysate, showing a 68 KDa band.

2.5 | Characterization of anti-RAI1 and anti-TCF20 antibodies

For expression analysis, we used a rabbit anti-RAI1 antibody (developed in-house) (Huang et al., 2016) that recognizes a highly conserved RPDGPADPAKQGPLRTSAR sequence in mouse RAI1 (aa 1738–1756), human RAI1 (aa 1756–1774, 100% identical), and marmoset RAI1 (aa 1753–1771). Note that the third proline at aa 1760 in the mouse epitope was replaced by leucine in marmoset RAI1. We previously validated the specificity of anti-RAI1 antibody using western blotting and immunofluorescent staining in the brains of *Rai1* knockout mice (Huang et al., 2016). For biochemistry, we used an anti-RAI1 antibody from Abcam (see Section 2.3). For TCF20, we used a rabbit anti-TCF20 antibody (Sigma, sab2106444) that recognizes the HYPCAIDAD-CLLHEENFSVRCPKHKPPLPCPLPPLQNKTAKGSLSTEQSE sequence, which is identical in human TCF20 (aa 1909–1958), marmoset TCF20 (aa 1901–1959), and mouse TCF20 (aa 1936–1985). The specificities

10969861, 2024, 1, Downloaded from https://onlinelibrary.wiley.com/doi/10.1002/cne.25589 by Cochrane Canada Provision, Wiley Online Library on [27/01/2024]. See the Terms and Conditions (https://onlinelibrary.wiley.com/terms-and-conditions) on Wiley Online Library for rules of use; OA articles are governed by the applicable Creative Commons License

of the RAI1 and TCF20 antibodies were validated by our CRISPR-mediated *RAI1*-KO and *TCF20*-KO cells. The specificities of all other antibodies were tested by the suppliers.

2.6 | Cell culture and plasmid transfection experiments

Human HEK293A cells (American Type Culture Collection, CRL-1573) were cultured in Dulbecco's Modified Eagle's Medium with GlutaMAX Supplement (Gibco) supplemented with nonessential amino acids, 10% Fetalgro, and 1% penicillin/streptomycin. Cells were split every 2–3 days using 0.25% trypsin (Gibco). For transfection, PEI 25K (Polysciences, 23966-1) was used according to the manufacturer's instructions.

2.7 | Immunoprecipitation and western blotting assays

For immunoprecipitation using cell lysates, cells were harvested in TNN lysis buffer (50 mM Tris-HCl at pH = 7.4, 250 mM NaCl, 5 mM EDTA at pH = 8.0, 0.5% Nonidet P-40) with 1 mM Na_3VO_4 (Fisher AAJ60191AD), 50 mM NaF, and protease inhibitor cocktail (SIGMA P8849). The lysates were then sonicated and clarified by centrifugation at 14,000 rpm at 4°C. Following a BCA assay, the protein concentration of the supernatant was measured, after which the samples were either stored at −20°C or processed through the following steps. To pulldown FLAG-tagged RAI1, control IgG (Fisher 10500C), or FLAG antibody was preincubated with protein A/G magnetic beads (Fisher PI88803) for 1 h at 4°C and then incubated with protein lysates overnight at 4°C. The beads were washed three times with TNN lysis buffer, once with 0.5 M LiCl buffer, and washed two more times with TNN lysis buffer. The beads were then boiled at 95°C in 4X SDS sample buffer and analyzed by western blotting.

For immunoprecipitation using mouse and marmoset cortices, tissues were lysed in radioimmune precipitation assay (RIPA) buffer (50 mM Tris at pH = 8.0, 150 mM NaCl, 0.5% sodium deoxycholate, 1% NP-40, and 0.1% SDS) with 1 mM Na_3VO_4 (Fisher AAJ60191AD), 50 mM NaF, and protease inhibitor cocktail (SIGMA P8849). The lysates were then sonicated and clarified by centrifugation at 14,000 rpm at 4°C. Control IgG (Fisher 10500C), RAI1, or TCF20 antibody was preincubated with protein A/G magnetic beads (Fisher PI88803) for 1 h at 4°C and then incubated with protein lysates overnight at 4°C. The beads were washed three times with RIPA buffer, once with 0.5 M LiCl buffer, and washed two more times with RIPA buffer. The beads were then boiled at 95°C in 4X SDS sample buffer and analyzed by western blotting with 10% input lysates prepared in 4X SDS sample buffer.

To perform a western blotting assay, an equal amount of protein lysates in 4X SDS sample buffer was denatured at 95°C for 5 min, fractionated by SDS-PAGE, and then electrotransferred to an Immobilon-FL PVDF membrane. The membranes were blocked in 5% milk in TBS for 30 min at room temperature and then incubated with primary antibodies in TBS containing 0.05% Tween 20 (TBS-T) with 5% bovine serum albumin overnight at 4°C. The next day, the membranes were washed with TBS-T and incubated with either horseradish peroxidase (HRP) or fluorescent secondary antibodies for 1 h at room temperature. Finally, membranes incubated with HRP-conjugated secondary antibody were developed with enhanced chemiluminescent substrate and scanned using a Bio-Rad ChemiDoc imager. Membranes incubated with fluorescent secondary antibodies were directly imaged with the Bio-Rad ChemiDoc imager. GAPDH was used as a loading control.

2.8 | Quantitative reverse transcription polymerase chain reaction

To extract total RNA, cells were harvested in TRizol reagent (Thermo-Fisher Scientific). Chloroform was added to the samples for phase separation, leaving RNA in the aqueous phase. After transferring the aqueous phase into a fresh Eppendorf tube, RNA was precipitated by mixing with isopropyl alcohol. The precipitated RNA was washed once with 75% ethanol and redissolved in nuclease-free water. The total RNAs from three biological replicas were used. The mRNA was reverse-transcribed with the SuperScript III First-Strand Synthesis System (Thermo-Fisher Scientific). Quantitative reverse transcription polymerase chain reactions were conducted using SsoFast EvaGreen Supermix (Bio-Rad) on a Real-Time PCR Detection System (Bio-rad).

2.9 | Image acquisition

Images were taken at 1024 × 1024 resolution using an Olympus FV-1000 confocal laser scanning microscope with 20x and 40x (NA 0.85 and 1.3, respectively). Stacks were taken with a step size of 1.0 μm, and images were acquired as a stack with at least 11 optical sections. Fiji ImageJ was used for image analysis and quantification. For most protein markers, the immunopositive cells from the whole field of 10 μm thick confocal images were manually counted. Binary and Analyze Particle functions were applied for NEUN staining (particle size greater than 25 μm^2). For immunopositive cells in $RAI1^+$ triangle patches, we counted the signals within the patch only (percentage of $RAI1^+$ cells that express specific markers). To exclude nonspecific signals, we compared images labeled with each antibody with images taken from fluorescent spectrums without secondary antibody staining (for us to evaluate autofluorescence background signals). For p-HH3 staining, only signals above the ventricular zone that were colocalized with DAPI were counted.

2.10 | Statistical analyses

All data were statistically analyzed using GraphPad Prism 10 software, and *p*-values less than .05 were considered significant. The levels

10969861, 2024, 1, Downloaded from https://onlinelibrary.wiley.com/doi/10.1002/cne.25589 by Cochrane Canada Provision, Wiley Online Library on [27/01/2024]. See the Terms and Conditions (https://onlinelibrary.wiley.com/terms-and-conditions) on Wiley Online Library for rules of use; OA articles are governed by the applicable Creative Commons License

of significance are indicated as follows: * < .05; ** < .01; *** < .001; and **** < .0001. Statistical analysis was performed using Student's *t*-test or one-way analysis of variance (ANOVA). A *p*-value of < .05 was considered statistically significant.

3 | RESULTS

3.1 | Neocortical distributions of RAI1 in newborn marmosets and mice

Rodents and primates last shared a common ancestor 83 million years ago (Mitchell & Leopold, 2015). Therefore, while RAI1 protein sequences in marmosets and mice are remarkably similar (81% identity), their neural distributions have likely diverged during neocortical evolution. The childhood onset of SMS symptoms suggests that the distribution of RAI1 in the neonatal brain is relevant to disease manifestation. To test this conjecture, we performed immunocytochemistry and compared the expression profiles of RAI1 in newborn marmosets and mice (P0-P5) (Figure 1a, see Figure S1 for illustrations of neuroanatomical positions). We focused on the prefrontal cortex, given that the retinoic acid-related genes are preferentially expressed in this structure in developing fetal human and macaque brains (Shibata et al., 2021), and our finding that *Rai1* haploinsufficiency in mice causes reductions in the dendritic spine density of prefrontal pyramidal neurons (Huang et al., 2018). We first examined the cortical ventricular zone, where an abundance of dividing neural precursor cells and radial glial cells reside, to determine whether marmoset RAI1 is enriched in proliferating cells or postmitotic neurons. We performed immunostaining using an anti-RAI1 antibody previously validated using *Rai1* knockout mice with western blots and immunostaining (Huang et al., 2016). Immunostaining in newborn marmosets revealed that only 10.5% (± 1.4%) phospho-histone H3-positive (p-HH3$^+$) proliferating cells near the ventricular zone show RAI1 immunoreactivity (Figure 1a). Similarly, only 12.9% (± 5.5%) of p-HH3$^+$ cells in the newborn mouse brains are RAI1-positive (Figure 1b), suggesting that most RAI1$^+$ cells are post-mitotic. Previous findings showed that many mitotic cells in newborn primate cortices express GFAP (Levitt et al., 1981, 1983). We found that in the newborn marmosets, the majority (85.3% [± 6.2%]) of p-HH3$^+$ cells coexpress GFAP and 18.4% (± 4.9%) of p-HH3$^+$ cells coexpress a neural progenitor marker SRY-Box Transcription Factor 2 (SOX2) (Figure S2a,b) (Graham et al., 2003). In mice, we found that 22.6% (± 7.0%) of p-HH3$^+$ cells coexpress GFAP and 30.0% (± 4.0%) of p-HH3$^+$ cells coexpress SOX2 (Figure S2c,d). By contrast, the p-HH3$^+$ cells do not coexpress an endothelial marker CD31 (Figure S2a,c). These data suggest that the p-HH3$^+$ cells are likely radial glial and neural progenitor cells (Homman-Ludiye et al., 2012; McDermott & Lantos, 1989; Rash et al., 2019). The observation of fewer proliferating GFAP$^+$ cells in mice is consistent with the fact that mouse GFAP is only expressed in radial glial cells during astrogenesis, while primate GFAP is additionally expressed in additional types of mitotic cells including basal radial glial cells (Levitt & Rakic, 1980). These findings are consistent with our previous observations that most proliferating cells that express p-HH3 in the embryonic mouse brain do not express RAI1 (Huang et al., 2016).

To determine whether marmoset RAI1 is enriched in neurons, we performed immunostaining and found that 54.6% (± 5.8%) of NEUN$^+$ neurons in the newborn marmoset prefrontal cortex and 78.9% (± 3.4%) of NEUN$^+$ neurons in the newborn mouse prefrontal cortex expressed RAI1 (Figure 1c,d,k). A subset of RAI1$^+$ cells coexpress astrocytic markers GFAP and S100β in newborn marmosets and mice (Figure 1e,f). Cell counts revealed that 15.7% (± 6.5%) of S100β^+ astrocytes in newborn marmosets and 8.3% (± 4.1%) of S100β^+ astrocytes in newborn mice express RAI1 (Figure 1e,f,l). These data suggest that during the neonatal stage, RAI1 is expressed in a higher percentage of neurons in mice than in marmosets. RAI1 is also more enriched in neurons than in astrocytes in both species.

The enriched RAI1 expression in neurons led us to profile the expression of RAI1 in excitatory and inhibitory neurons. Immunostaining using cell-type–specific markers revealed that in newborn marmosets, 48.3% (± 2.1%) of neuronal differentiation 2-expressing (NEUROD2$^+$) excitatory neurons (Figure 1g,m) and 44.5% (± 4.3%) of glutamate decarboxylase-expressing (GAD67$^+$) GABAergic neurons (Figure 1i,n) expressed RAI1. In newborn mice, 67.4% (± 1.6%) of NEUROD2$^+$ excitatory neurons (Figure 1h,m) and 51.6% (± 2.3%) of GAD67$^+$ GABAergic neurons (Figure 1j,n) expressed RAI1. Overall, we found that the percentage of neurons expressing RAI1, especially in excitatory neurons, is higher in newborn mice than in newborn marmosets.

3.2 | RAI1 expression pattern in upper layers of newborn marmoset prefrontal cortex

In newborn marmosets, we noticed higher expression levels of RAI1 in the upper cortical layers. Interestingly, we found patches of RAI1$^+$ cells arranged in a reverse triangle pattern localized mostly within layers II and III (Figure 2a and Figure S3a), as shown by the costaining of TBR1 that labels several cortical layers below layer I in the postnatal cortex (Figure 2b) (Co et al., 2022; Englund et al., 2005). To examine whether or not RAI1$^+$ cells at the upper edges of these triangle patches are localized within layer I, we costained REELIN to label cortical layer I Cajal–Retzius cells (Ogawa et al., 1995). We found that some RAI1$^+$ cells near the upper edges of the triangle patches are intermingled but are distinct from the REELIN-expressing Cajal–Retzius cells (Figure 2c), suggesting that the majority of the RAI1$^+$ patches are within layers II/III. Quantification showed that 35.6% (± 5.7%) of RAI1$^+$ cells within the triangle patches coexpress N-Methyl-D-aspartic acid receptor 1 (NR1) (Figure 2d,g). Within these triangle patches, 91.9% (± 1.9%) of RAI1$^+$ cells coexpress a neuronal marker NEUN and 9.5% (± 4.0%) of RAI1$^+$ cells coexpress GFAP (Figure 2e,h). This suggests that RAI1$^+$ cells within the layer II/III triangle patches are predominantly neurons. *Rai1* was first identified as a retinoic acid-inducible gene (Imai et al., 1995). We stained for RARα and found that 42.1% (± 10.1%) of RAI1$^+$ neurons within the triangles express RARα (Figure 2f,i). These data suggest that the reverse triangle patches of

10969861, 2024, 1, Downloaded from https://onlinelibrary.wiley.com/doi/10.1002/cne.25589 by Cochrane Canada Provision, Wiley Online Library on [27/01/2024]. See the Terms and Conditions (https://onlinelibrary.wiley.com/terms-and-conditions) on Wiley Online Library for rules of use; OA articles are governed by the applicable Creative Commons License

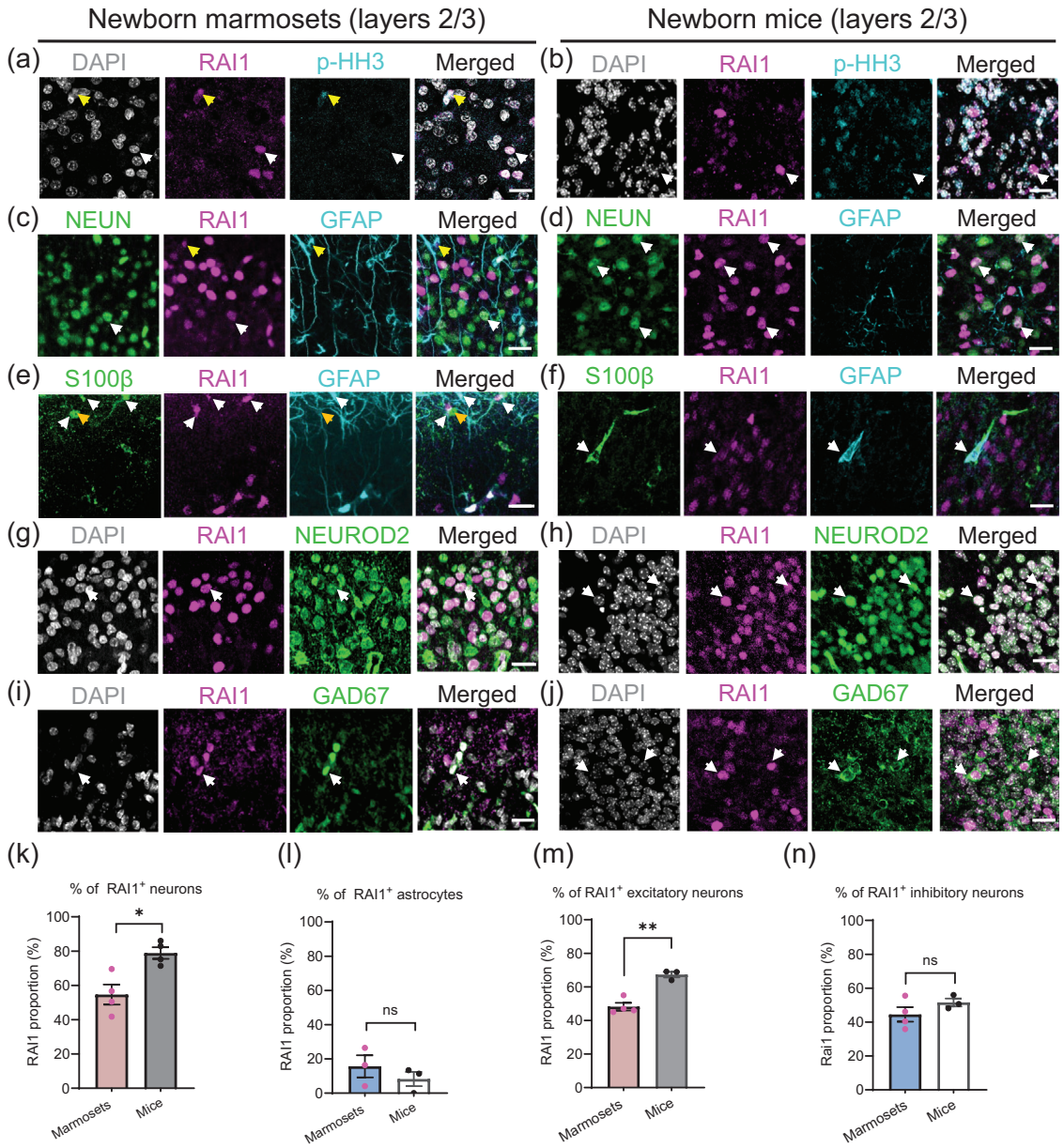

FIGURE 1 Immunofluorescence staining showing the cortical distribution of RAI1 in newborn marmosets and mice. (a) Most p-HH3$^+$ proliferating cells in the ventricular zones of neonatal marmoset cortices do not coexpress RAI1 (yellow arrows indicate a p-HH3$^+$ cell that coexpress RAI1; white arrows indicate a RAI1$^+$ cell that does not express p-HH3). (b) In the ventricular zone of newborn mice, most RAI1$^+$ cells (white arrows) do not express p-HH3. (c) In newborn marmosets, RAI1 is expressed in NEUN$^+$ neurons (white arrows) and to a lesser extent, GFAP$^+$ astrocytes (yellow arrows). (d) In newborn mice, RAI1 is primarily enriched in NEUN$^+$ neurons (white arrowheads) but absent in most GFAP$^+$ astrocytes. (e) In newborn marmosets, RAI1 is expressed in a subset of S100β^+/GFAP$^+$ astrocytes (white arrows). (f) In newborn mice, RAI1 is occasionally detected in the S100β^+/GFAP$^+$ astrocytes (white arrows). (g) In newborn marmosets, RAI1 is expressed in a subset of NEUROD2$^+$ excitatory neurons (white arrows). (h) In newborn mice, RAI1 is expressed in a subset of NEUROD2$^+$ excitatory neurons (white arrows). (i) In newborn marmosets, RAI1 is expressed in a subset of GAD67$^+$ GABAergic neurons (white arrows). Female animals are in pink and animals without identified sexes are in black. (j) In newborn mice, RAI1 is expressed in a subset of GAD67$^+$ GABAergic neurons (white arrows). Scale bar: 20 μm (a–j). (k) Quantification shows that the percentage of NEUN$^+$ neurons expressing RAI1 is higher in newborn mice than in newborn marmosets (shown are mean ± SEM, unpaired *t*-test, $^*p = .01$, $n = 3$–4 samples/species). (l) Quantification shows that the percentage of S100β^+ astrocytes expressing RAI1 is similar in newborn mice and marmosets (shown are mean ± SEM, unpaired *t*-test, $p = .39$, $n = 3$ samples/species). (m) Quantification shows that the percentage of NEUROD2$^+$ excitatory neurons expressing RAI1 is higher in newborn mice than in marmosets (shown are mean ± SEM, unpaired *t*-test, $^{**}p = .001$, $n = 3$–4 samples/species). (n) Quantification shows that the percentage of GAD67$^+$ inhibitory neurons expressing RAI1 is similar in newborn mice and marmosets (shown are mean ± SEM, unpaired *t*-test, $p = .21$, $n = 3$–4 samples/species).

10969861, 2024, 1, Downloaded from https://onlinelibrary.wiley.com/doi/10.1002/cne.25589 by Cochrane Canada Provision, Wiley Online Library on [27/01/2024]. See the Terms and Conditions (https://onlinelibrary.wiley.com/terms-and-conditions) on Wiley Online Library for rules of use; OA articles are governed by the applicable Creative Commons License

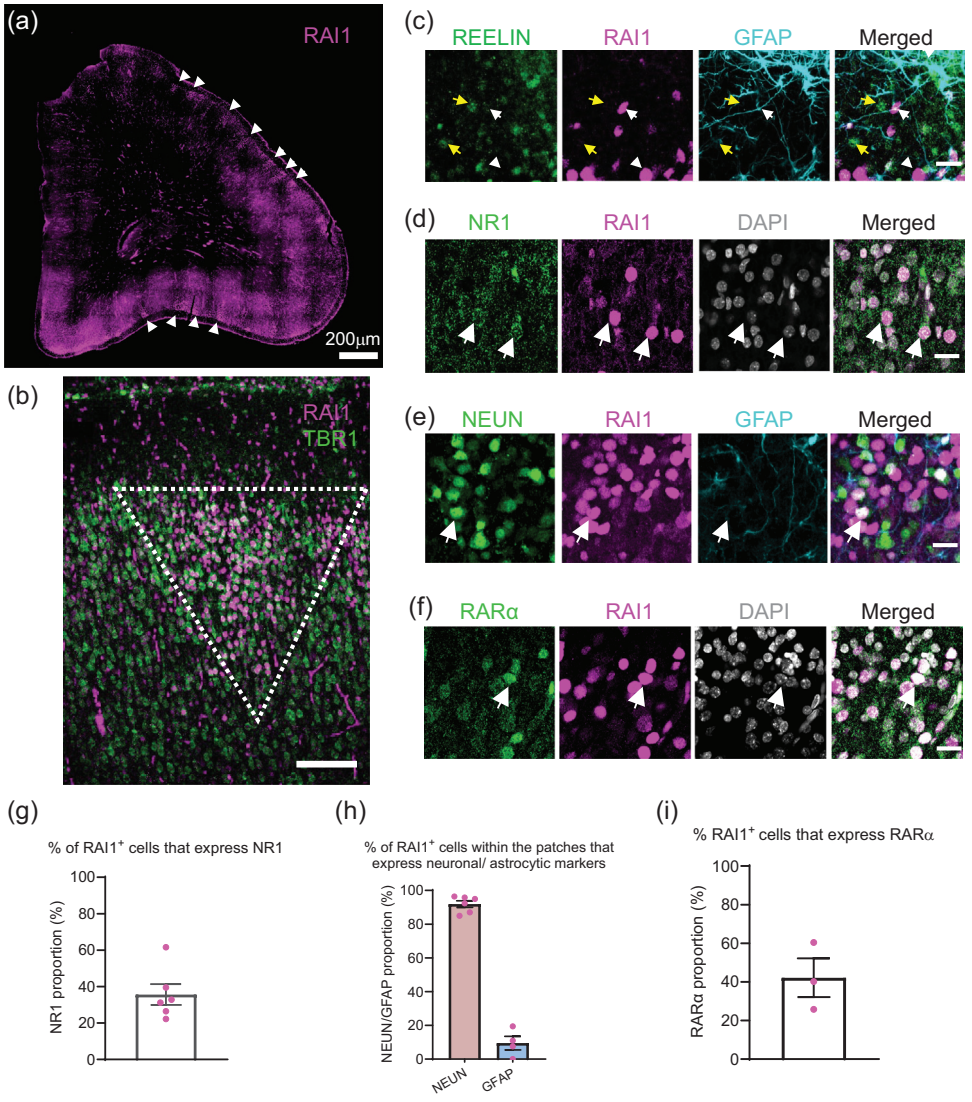

FIGURE 2 Immunofluorescence staining showing RAI1 distribution in the upper layers of newborn marmoset cortex. (a) RAI1 (magenta) expression in the newborn marmoset prefrontal cortex. White arrowheads indicate clusters of RAI1$^+$ triangle patches. Scale bar: 200 μm. (b) A triangle patch of RAI1$^+$ cells (white dashed triangle, scale bar: 100 μm) located in the TBR1-expressing domain right below layer I in the newborn marmoset prefrontal cortex. (c) At the upper edges of the RAI1$^+$ triangle patches, RAI1 (white arrows) is largely absent from the REELIN$^+$ Cajal–Retzius cells (yellow arrows). Scale bar: 20 μm. (d) A single optical plane showing that within the RAI1$^+$ triangle patches, some RAI1$^+$ cells show colocalization with NR1. Scale bar: 20 μm. (e) Within the RAI1$^+$ patches, RAI1 mostly colocalizes with NEUN but not GFAP, consistent with a neuronal identity. Scale bar: 20 μm. (f) Within the RAI1$^+$ patches, RAI1 shows some colocalization with RARα-expressing cells. Scale bar: 20 μm. (g) Quantification shows the percentage of RAI1$^+$ cells within triangle patches that express NR1 in newborn marmosets. (h) Quantification shows the percentage of RAI1$^+$ cells within triangle patches that express NEUN or GFAP in newborn marmosets. (i) Quantification shows the percentage of RAI1$^+$ cells within triangle patches that express RARα in newborn marmosets.

cells near the cortical surface comprise RAI1$^+$ neurons, some coexpress RARα, likely resulting from the high retinoic acid concentration in the medial prefrontal cortex.

The primate plexiform layer contains GFAP$^+$ interlaminar astrocytes, which represent a group of distinct primate-specific glial cells characterized by their long, fine, unbranched processes (often greater than 300 μm in length) extending toward layers II–IV (Falcone et al., 2019; Munoz et al., 2021; Oberheim et al., 2009). We found that 30.1% (± 4.6%) of GFAP$^+$ interlaminar astrocytes express RAI1, with their somas juxtaposed to, and their long processes extending away from, the pial surface (Figure 3a; a reconstructed RAI1$^+$/GFAP$^+$ interlaminar astrocyte is shown on the left). Another group of primate-specific cells enriched in the prefrontal cortex are the lateral ganglionic eminence-derived MEIS2$^+$ GABAergic neurons, which are absent from the corresponding regions in mice (Kita et al., 2021; Schmitz et al., 2022). We found that 68.7% (± 2.1%) of MEIS2$^+$ neurons in layers II/III of newborn marmoset prefrontal cortices express RAI1 (Figure 3b), in stark contrast to the absence of RAI1$^+$/MEIS2$^+$ neurons in the same region in newborn mice (Figure 3b). Compared to the more selective RAI1 expression pattern in newborn marmosets, RAI1 expression is

10969861, 2024, 1, Downloaded from https://onlinelibrary.wiley.com/doi/10.1002/cne.25589 by Cochrane Canada Provision, Wiley Online Library on [27/01/2024]. See the Terms and Conditions (https://onlinelibrary.wiley.com/terms-and-conditions) on Wiley Online Library for rules of use; OA articles are governed by the applicable Creative Commons License

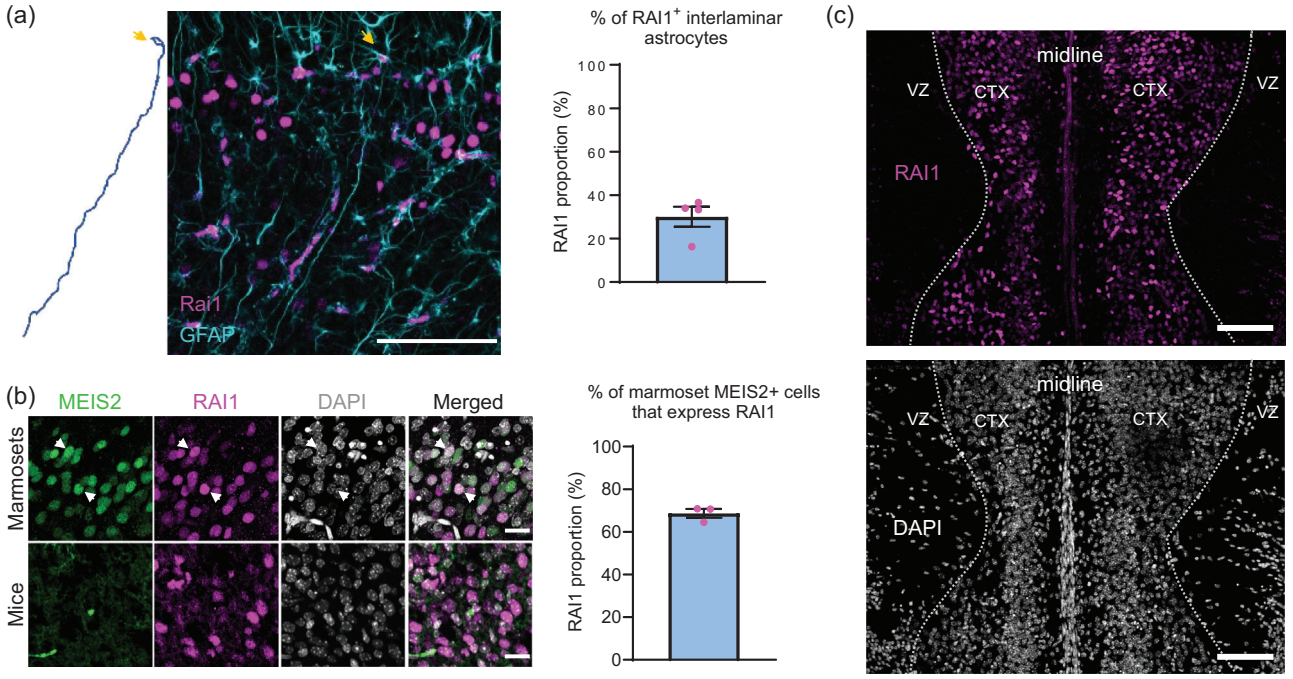

FIGURE 3 Immunofluorescence staining showing expression of RAI1 in primate-specific cell types in newborn marmosets. (a) GFAP and RAI1 expression (middle) and a reconstructed GFAP$^+$/RAI1$^+$ interlaminar astrocyte (left, soma indicated by a yellow arrow) localized within the superficial prefrontal layer of a newborn marmoset. Quantification is shown on the right. Scale bar: 100 μm. (b) Within layers II/III of a newborn marmoset, primate-specific MEIS2$^+$ GABAergic neurons express RAI1 (top panel, white arrowheads indicate double-positive cells). By contrast, newborn mice lack MEIS2$^+$ GABAergic neurons in the corresponding brain region (bottom panel). Quantification is shown on the right. Scale bars: 20 μm. (c) In the prefrontal cortex of newborn mice, RAI1 is distributed throughout the cortical layers (upper panel DAPI in gray at the lower panel). CTX, cortex; VZ, ventricular zone. Scale bars: 20 μm.

more uniformly distributed across all cortical layers in newborn mice (Figure 3c), adult marmosets (Figure S3b), and adult mice (Figure S3c). These data suggest that in prefrontal layers II/III of newborn marmosets, RAI1 is expressed in more selective groups of cells, including several primate-specific cell types without mouse homologs.

3.3 | Neocortical distributions of RAI1 in adult marmosets and mice

In previous work, we found that continuous RAI1 function is required in the adult mouse brain (Javed et al., 2021). Therefore, we characterized the expression pattern of RAI1 in the prefrontal cortices of adult marmosets (5-year-old) and adult mice (8-week-old). In adult marmoset cortices, 86.4% (± 1.2%) of NEUN$^+$ neurons (Figure 4a,i) and 8.4% (± 4.3%) of S100β^+ astrocytes express RAI1 (Figure 4c,j). Among neurons, RAI1 is detected in 57.1% (± 10.0%) of CAMKII$^+$ excitatory neurons (Figure 4e,k) and 36.5% (± 6.8%) of GAD67$^+$ inhibitory neurons (Figure 4g,l). In the adult mouse brain, we found that 77.8% (± 3.9%) of NEUN$^+$ neurons (Figure 4b,i) and 9.6% (± 1.3%) of S100β^+ astrocytes (Figure 4d,j) express RAI1. Cell counts revealed that RAI1 is expressed in 57.5% (± 1.8%) of CAMKII$^+$ excitatory neurons (Figure 4f,k) and 44.3% (± 2.4%) of GAD67$^+$ inhibitory neurons (Figure 4h,l). These data indicate that excitatory and inhibitory neurons in adult marmosets and mice show a similar RAI1 expression profile. Interestingly, we found a significant difference in the mean percentages of RAI1$^+$/NEUN$^+$ (double-positive) neurons across species and age groups (p = .0131, Welch's ANOVA). The percentage of neurons that express RAI1 increased by 31.75% in adult marmosets when compared to newborn marmosets (p = .027, Dunnett's T3 multiple comparisons test). This pattern of increased RAI1 expression during neural maturation was not observed in excitatory neurons (Welch's ANOVA).

3.4 | RAI1 forms an evolutionarily conserved and developmentally stable protein complex with TCF20, PHF14, and HMG20A in mouse and marmoset cortices

RAI1 is structurally paralogous to TCF20, a chromatin-binding protein that potentially originated from a duplication event of the ancestral *Rai1* gene in early vertebrate evolution after vertebrates branched off from insects (Darvekar et al., 2013). In humans, pathogenic variants or deletion of *TCF20* causes *TCF20*-associated neurodevelopmental disorder, which is characterized by multiple phenotypes resembling those seen in SMS, including delayed motor reactions, autism, intellectual impairment, seizures, and sleep disturbances (Babbs et al., 2014;

10969861, 2024, 1, Downloaded from https://onlinelibrary.wiley.com/doi/10.1002/cne.25589 by Cochrane Canada Provision, Wiley Online Library on [27/01/2024]. See the Terms and Conditions (https://onlinelibrary.wiley.com/terms-and-conditions) on Wiley Online Library for rules of use; OA articles are governed by the applicable Creative Commons License

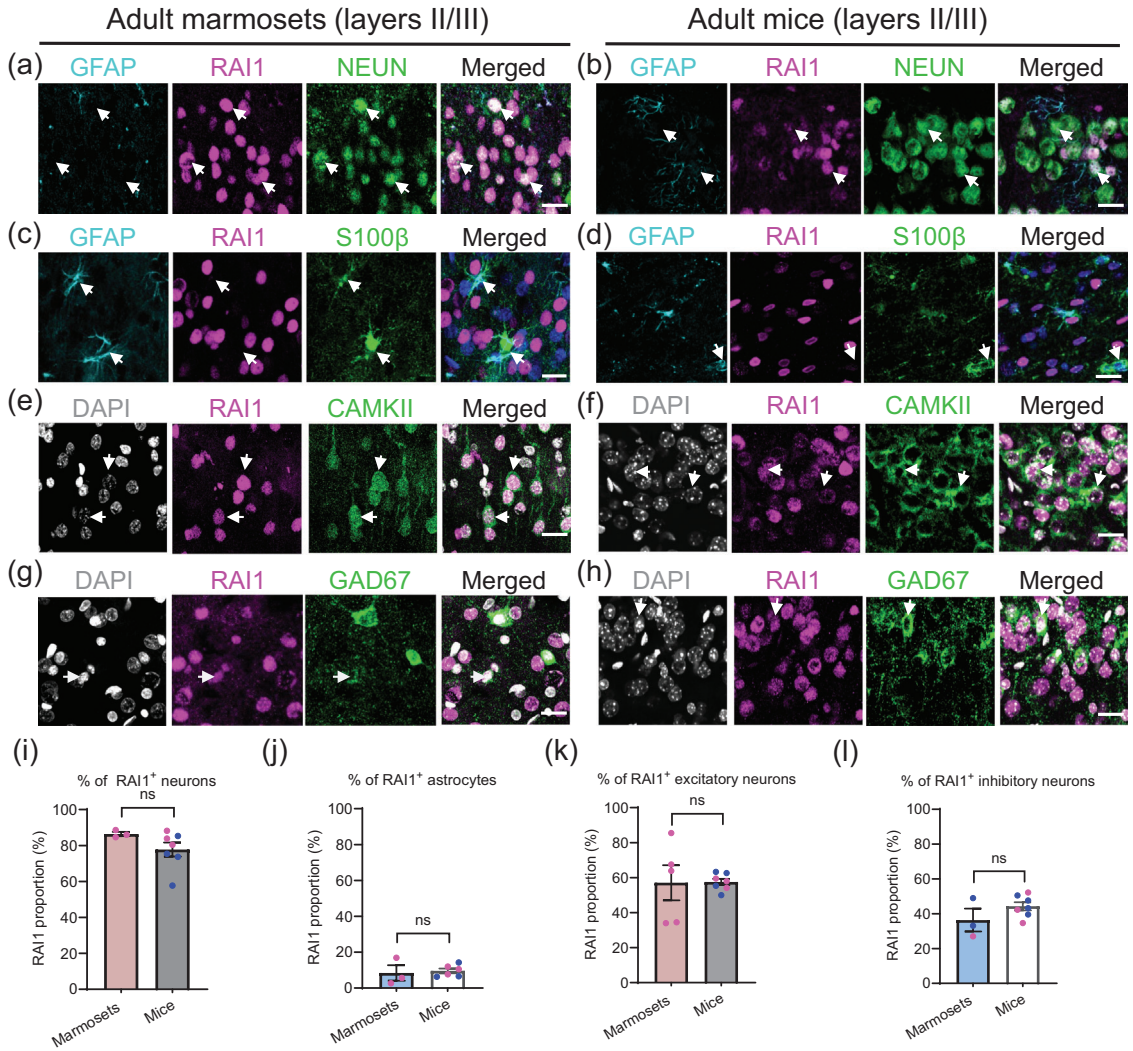

FIGURE 4 Immunofluorescence staining showing the cortical distribution of RAI1 in adult marmosets and mice. (a) In adult marmosets, RAI1 is expressed in most NEUN$^+$ neurons (white arrows) but absent in most GFAP$^+$ astrocytes. (b) In adult mice, RAI1 is expressed in most NEUN$^+$ neurons (white arrows) but absent in most GFAP$^+$ astrocytes. (c) In adult marmosets, RAI1 is largely absent in S100β^+/GFAP$^+$ astrocytes (white arrows). (d) In adult mice, RAI1 is absent in S100β^+/GFAP$^+$ astrocytes (white arrows). (e) In adult marmosets, RAI1 is expressed in a subset of CAMKII$^+$ excitatory neurons (white arrows). (f) In adult mice, RAI1 is expressed in a subset of CAMKII$^+$ excitatory neurons (white arrows). (g) In adult marmosets, RAI1 is expressed in a subset of GAD67$^+$ GABAergic neurons (white arrows). (h) In adult mice, RAI1 is expressed in a subset of GAD67$^+$ GABAergic neurons (white arrows). Scale bars: 20 μm (a–h). (i) Quantification shows that the percentage of NEUN$^+$ neurons expressing RAI1 in adult mice and marmosets is similar (shown are mean ± SEM, unpaired *t*-test, $p = .07$). Male animals are in blue and female animals are in pink. (j) Quantification shows that the percentage of S100β^+ astrocytes expressing RAI1 in adult mice and marmosets is similar (shown are mean ± SEM, unpaired *t*-test, $p = .82$). (k) Quantification shows that the percentage of CAMKII$^+$ excitatory neurons expressing RAI1 in adult mice and marmosets are similar (shown are mean ± SEM, unpaired *t*-test, $p = .96$). (l) Quantification shows that the percentage of GAD67$^+$ inhibitory neurons expressing RAI1 in adult mice and marmosets are similar (shown are mean ± SEM, unpaired *t*-test, $p = .18$).

Lelieveld et al., 2016; Schafgen et al., 2016; Torti et al., 2019; Upadia et al., 2018; Vetrini et al., 2019). In addition, *de novo* 22q13.2 duplication containing *TCF20* causes a neurodevelopmental disorder with disease traits mirroring patients carrying *TCF20* deletions (Levy et al., 2021). These findings highlight the importance of *TCF20* dosage for brain function. Using immunolabeling, we first tested whether RAI1 and TCF20 are coexpressed in the cortices of marmosets and mice. Quantification revealed that in marmoset cortices, 71.2% (± 1.8%) of RAI1$^+$ cells express TCF20 and 78.9 (± 6.1%) of TCF20$^+$ cells express Rai1 (Figure 5a,c). Similarly, in mouse cortices, 70.7% (± 11.4%) of RAI1$^+$ cells express TCF20 and 74.8% (± 8.8%) of TCF20$^+$ cells express Rai1 (Figure 5b,c). The coexpression profiles of RAI1 and TCF20 prompted us to test their molecular interactions in vivo. It was previously reported that RAI1 forms a protein complex with TCF20 and two other chromatin-interacting proteins, PHF14 and HMG20A, in human cells (Eberl et al., 2013; Hein et al., 2015) and adult mouse brains (Zhou et al., 2022). To study the endogenous interaction of RAI1 and TCF20 in newborn mouse cortices, we used a previously generated mouse model that expresses RAI1–FLAG fusion protein (Huang et al., 2016). Immunoprecipitation using an anti-RAI1 antibody revealed that endogenous RAI1 interacts with TCF20 in newborn mouse cortices (top panel, Figure 5d). The successful pull-down of RAI1 was validated

10969861, 2024, 1, Downloaded from https://onlinelibrary.wiley.com/doi/10.1002/cne.25589 by Cochrane Canada Provision, Wiley Online Library on [27/01/2024]. See the Terms and Conditions (https://onlinelibrary.wiley.com/terms-and-conditions) on Wiley Online Library for rules of use; OA articles are governed by the applicable Creative Commons License

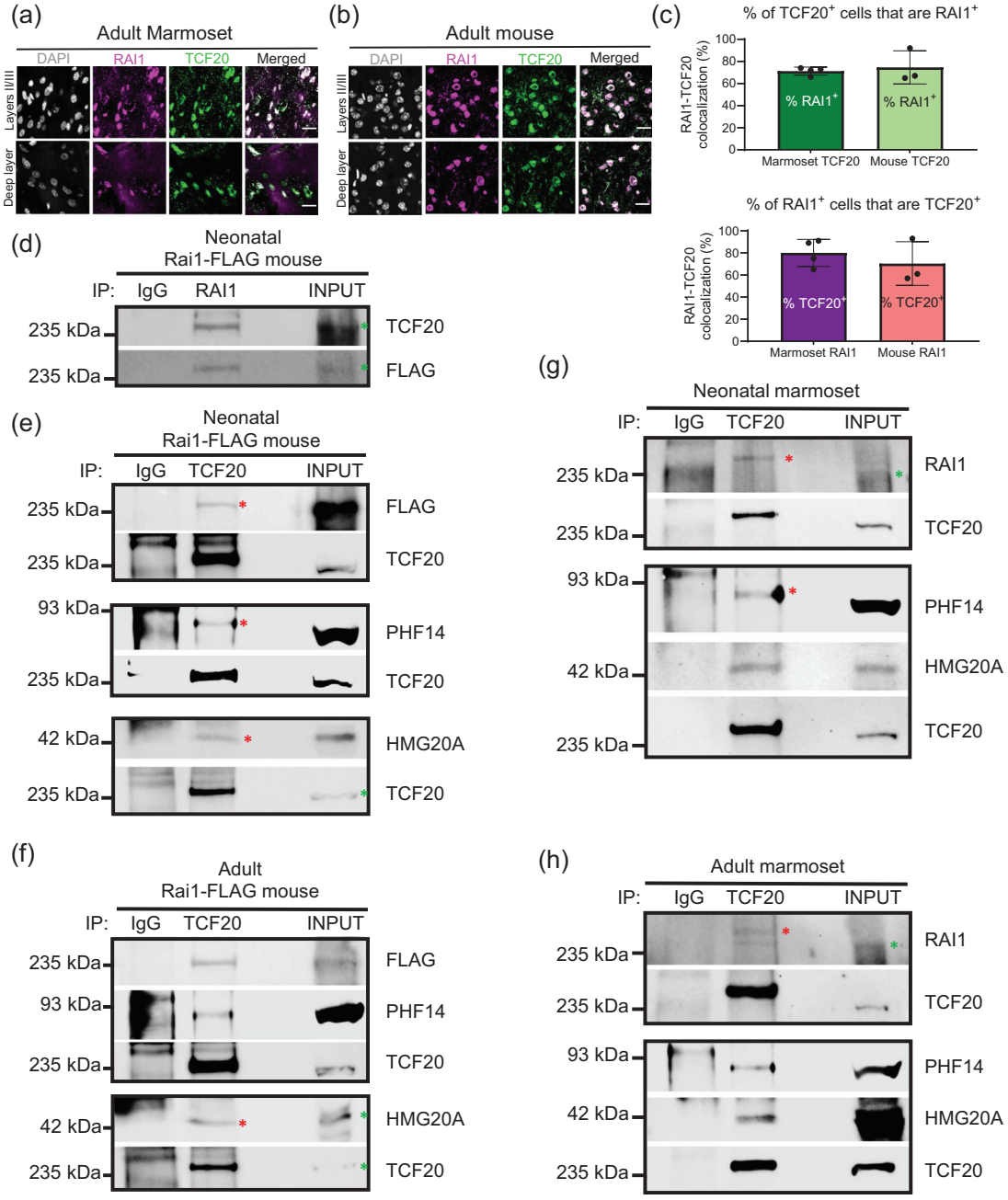

FIGURE 5 RAI1 and TCF20 are highly colocalized and form an evolutionarily conserved protein complex in the cortex. (a) Immunofluorescence staining shows that RAI1 and TCF20 are highly colocalized throughout all layers in the adult marmoset prefrontal cortex. Scale bars: 20 μm. (b) Immunofluorescence staining shows that RAI1 and TCF20 are highly colocalized throughout all layers in the adult mouse prefrontal cortex. Scale bars: 20 μm. (c) Quantification shows that more than 70% of TCF20$^+$ cells express RAI1 (top) and that more than 70% of RAI1$^+$ cells express TCF20 (bottom). (d) Top panel: immunoprecipitation using an anti-RAI1 antibody identifies RAI1–TCF20 interaction in cortical extracts of newborn Rai1-FLAG mouse. Bottom panel: western blotting using an anti-FLAG antibody confirms the successful pull-down of RAI1. (e) Immunoprecipitation experiments using an anti-TCF20 antibody show that TCF20 interacts with RAI1-FLAG (top panel), PHF14 (middle panel), and HMG20A (bottom panel) in cortical extracts of newborn Rai1-FLAG mice. Western blotting using an anti-TCF20 antibody confirms a successful pull-down of TCF20. (f) Immunoprecipitation experiments using an anti-TCF20 antibody show that TCF20 interacts with RAI1-FLAG (top panel), PHF14 (top panel), and HMG20A (bottom panel) in cortical extracts from adult Rai1-FLAG mice. Western blotting using an anti-TCF20 antibody confirms a successful pull-down of TCF20. (g) Immunoprecipitation experiments using an anti-TCF20 antibody show that TCF20 interacts with RAI1 (top panel), PHF14 (middle panel), and HMH20A (bottom panel) in cortical extracts of newborn marmosets. Western blotting using an anti-TCF20 antibody confirms a successful pull-down of TCF20. (h) Immunoprecipitation experiments using an anti-TCF20 antibody show that TCF20 interacts with RAI1 (top panel), PHF14, and HMG20A (bottom panels) in cortical extracts of adult marmosets. Western blotting using an anti-TCF20 antibody confirms a successful pull-down of TCF20. The positive bands of the immunoprecipitation reactions are marked with red asterisks and the input bands are marked with green asterisks (*). All immunoprecipitation experiments were performed two to three times (also see Figure S4). Note that some proteins showed increased molecular weight after IP enrichment, which is not uncommon in IP experiments. A potential explanation includes the enrichment of post-translationally modified proteins.

10969861, 2024, 1, Downloaded from https://onlinelibrary.wiley.com/doi/10.1002/cne.25589 by Cochrane Canada Provision, Wiley Online Library on [27/01/2024]. See the Terms and Conditions (https://onlinelibrary.wiley.com/terms-and-conditions) on Wiley Online Library for rules of use; OA articles are governed by the applicable Creative Commons License

with an anti-FLAG antibody (bottom panel, Figure 5d). This suggests that RAI1 and TCF20 interact during early cortical development. However, the same anti-RAI1 antibody was unable to pull down RAI1 from the adult mouse or marmoset brains. Therefore, an anti-TCF20 antibody was used to pull down the RAI1 protein complex from mouse and marmoset brains. We then performed the reciprocal experiment by pulling down endogenous TCF20 and found that TCF20 interacts with RAI1, PHF14, and HMG20A in newborn mouse cortices (Figure 5e). We also confirmed the presence of the RAI1–TCF20, PHF14, and HMG20A protein complex in adult mouse cortices (Figure 5f). Importantly, by performing TCF20 pull-down followed by western blotting assays, we demonstrated that RAI1, TCF20, PHF14, and HMG20A form a protein complex in newborn (Figure 5g) and adult (Figure 5h) marmoset cortices (also see Figure S4). These experiments extend previous findings and provide in vivo evidence that RAI1 forms a protein complex with TCF20, PHF14, and HMG20A in both mouse and marmoset cortices throughout development.

3.5 | Deletion and overexpression assays identify human TCF20 as a regulator of human RAI1 protein abundance

In a heteromeric protein complex, the protein abundance of each subunit is often coordinated (Taggart et al., 2020). To test if RAI1 maintains TCF20 abundance (and vice versa), we generated *RAI1* and *TCF20* knockout human 293A cells using the CRISPR gene editing technique. Specifically, two single guide (sg) RNAs were coexpressed with the CRISPR-associated protein 9 (Cas9) to induce *RAI1* or *TCF20* deletions (Figure 6a). In *RAI1* knockout (*RAI1*-KO) clones, western blotting confirmed that RAI1 protein levels were dramatically decreased (Figure 6b). However, the protein levels of TCF20 and two other RAI1-interacting proteins, PHF14 and HMG20A, remained unchanged upon *RAI1* deletion (Figure 6b,c). This suggests that RAI1 does not regulate the abundance of its interacting proteins, including TCF20, PHF14, and HMG20A in human cells.

We then deleted *TCF20* using a pair of sgRNAs (Figure 6d) and confirmed that TCF20 protein levels were significantly reduced (Figure 6e). Interestingly, RAI1 (but not PHF14 or HMG20A) protein levels were significantly reduced in *TCF20*-KO cells (Figure 6e,f). We found that *RAI1* mRNA levels were slightly increased in both *TCF20*-KO clones (Figure 6g), suggesting that *TCF20* ablation reduces the stability of RAI1 protein without reducing *RAI1* transcription. Finally, we showed that overexpression of TCF20 significantly increased RAI1 protein abundance (Figure 6h). By contrast, TCF20 overexpression did not affect the protein abundance of PHF14 or HMG20A (Figure 6i). Together, these data suggest that the stability of RAI1 protein is maintained by TCF20 but not vice versa.

4 | DISCUSSION

Mutations in genes that encode chromatin-interacting proteins have been frequently implicated in neurodevelopmental disorders (De Rubeis et al., 2014). This study delineates how the expression patterns and molecular interactions of RAI1, a chromatin-interacting protein mutated in SMS, have remained conserved or diverged during neocortical evolution. Notably, the results show that (a) in layers II/III of the prefrontal cortex in newborn marmosets, RAI1-expressing neurons show 40% colocalization with RARα and show a patchy expression pattern; (b) a higher percentage of excitatory neurons in newborn mice express RAI1 compared to excitatory neurons in newborn marmosets; (c) RAI1 is expressed in primate-specific cell types, including interlaminar astrocytes and MEIS2$^+$ GABAergic neurons within the superficial layers of the prefrontal cortex; (d) RAI1 forms an evolutionarily conserved protein complex with TCF20, PHF14, and HMG20A in the marmoset brain; and (e) TCF20 regulates RAI1 protein abundance but not vice versa. Collectively, these findings suggest that the expression pattern of RAI1 in the neocortex is more restricted in newborn primates than in newborn mice, and that the interaction of RAI1 with TCF20, PHF14, and HMG20A is highly conserved.

4.1 | Cellular distribution of RAI1 in primate and mouse prefrontal cortices

Human and mouse RAI1 are widely distributed within and outside the nervous system and yet, neurocognitive problems are among the most prominent features in SMS patients and *Rai1*$^{+/-}$ mice. For example, the majority of SMS patients show autistic features including social dysfunction at some point of their lives (Laje et al., 2010), while *Rai1*$^{+/-}$ mice show impaired social dominance in the tube test (Huang et al., 2018; Rao et al., 2017). Among the candidate brain regions impacted by RAI1 loss, the prefrontal cortex stands out given its roles in social dominance, recognition, and motivation (Chini & Hanganu-Opatz, 2021; C. Zhang et al., 2022). Our previous work revealed that *Rai1*$^{+/-}$ mice show decreased dendritic spine density in the medial prefrontal cortex, and that reduced social dominance in *Rai1*$^{+/-}$ mice can be partially rescued by optogenetically stimulating the same brain region (Huang et al., 2018). We previously performed ^{18}Fluoro-2-deoxyglucose positron emission tomography/computed tomography and found that mice with brain-specific *Rai1* ablation show reduced metabolic activity in the frontal cortex compared to control littermates (Y. T. Chang et al., 2022). Together, the data from clinical and animal studies suggest that loss of Rai1 leads to dysfunction of the prefrontal cortex.

This study showed that in the adult marmoset and mouse prefrontal cortex, most neurons (> 70%) express RAI1. Quantification revealed that RAI1 is expressed in a similar percentage of adult excitatory and inhibitory neurons in both species. While the function of neuronal RAI1 in primates remains to be determined, we have demonstrated that in mice, neuron-specific RAI1 loss induces SMS-like behavioral phenotypes (Huang et al., 2016). By contrast, we found that only ~9% of astrocytes in adult mice or marmosets express RAI1. Previous work showed that deleting *Rai1* from GFAP$^+$ astrocytes did not induce any detectable SMS-like disease features in mice (Huang et al., 2016), supporting the notion that RAI1 function is most critical in neurons.

10969861, 2024, 1, Downloaded from https://onlinelibrary.wiley.com/doi/10.1002/cne.25589 by Cochrane Canada Provision, Wiley Online Library on [27/01/2024]. See the Terms and Conditions (https://onlinelibrary.wiley.com/terms-and-conditions) on Wiley Online Library for rules of use; OA articles are governed by the applicable Creative Commons License

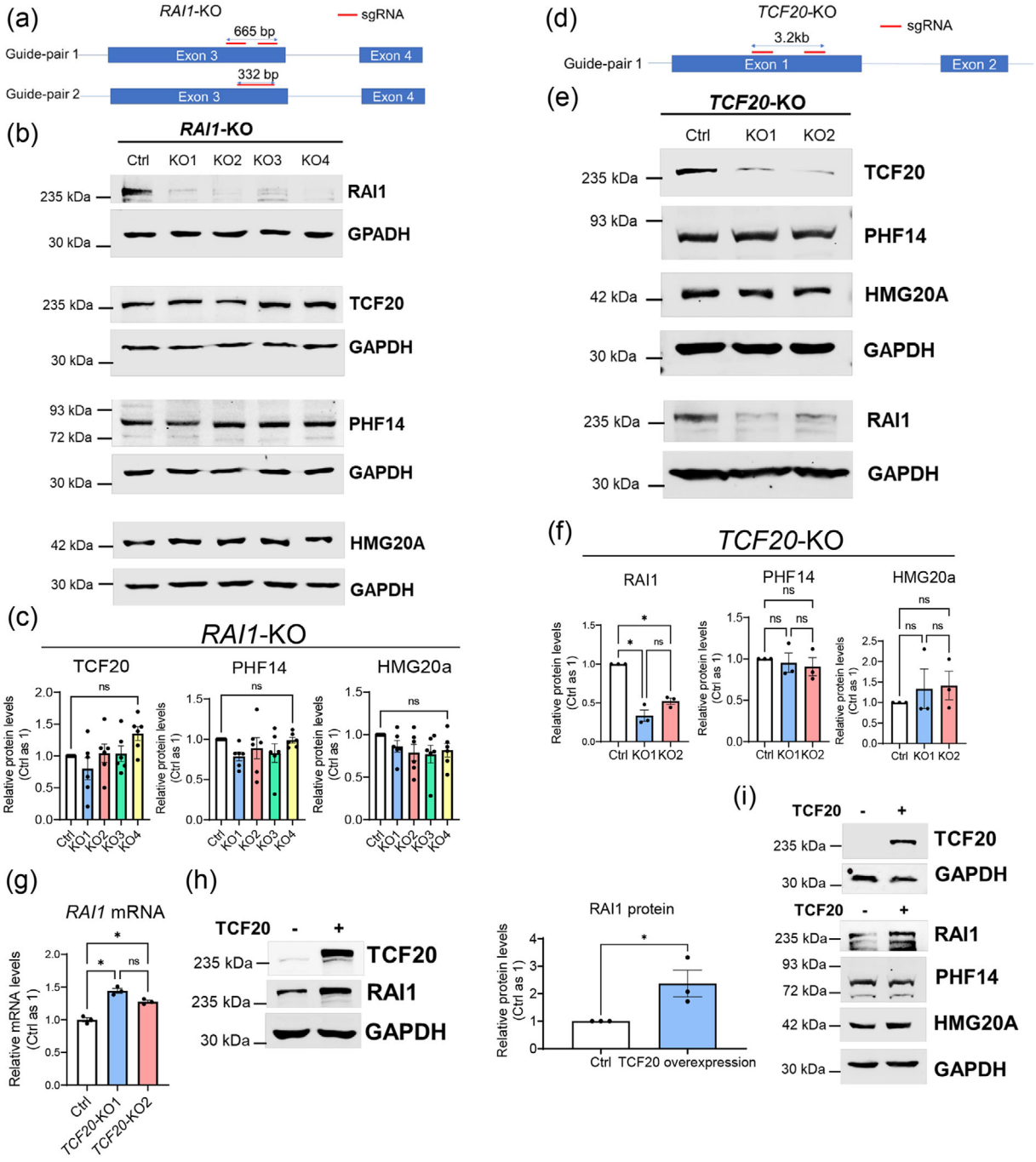

FIGURE 6 Human TCF20 bi-directionally regulates human RAI1 protein abundance. (a) Illustrations show two independent pairs of sgRNAs used to induce genetic deletion of human *RAI1*. (b) Four independent *RAI1*-knockout (KO) clones of human 293A cells were generated using two pairs of sgRNAs (guide-pairs). KO1 and KO2 were generated by guide-pair 1, while KO3 and KO4 were generated by guide-pair 2. Representative western blotting data show that RAI1 protein levels decrease in KO clones 1–4. By contrast, TCF20, PHF14, and HMG20A protein levels remain unchanged. (c) Quantification shows that in four different *RAI1*-KO clones, the protein levels of RAI1 (but not the other three RAI1-interacting proteins) decrease. $N = 6$ independent replications for each clone. ns: not significantly different, one-way ANOVA. (d) Illustration shows a pair of sgRNAs that induce *TCF20* deletion in human cells. (e) Western blotting assays show that endogenous TCF20 protein levels significantly decrease in two independent *TCF20*-KO clones, confirming successful *TCF20* knockout. RAI1 protein levels decrease, while PHF14 and HMG20A protein levels remain unchanged. (f) Quantification shows that in two independent *TCF20*-KO clones, the protein levels of RAI1 (but not PHF14 or HMG20A) decrease. $N = 3$ independent replications for each clone. $^*p < .05$, one-way ANOVA. (g) Quantitative RT-PCR shows that *RAI1* mRNA levels are slightly upregulated in *TCF20*-KO clones. $^*p < .05$, one-way ANOVA. (h) Left: western blotting data show that TCF20 overexpression increases RAI1 protein abundance. Right: quantification shows significantly increased RAI1 protein levels upon TCF20 overexpression. Three independent biological replicates, $^*p < .05$, unpaired *t*-test. (i) Western blotting shows that overexpressing TCF20 increases RAI1 protein levels but not PHF14 or HMG20A.

10969861, 2024, 1, Downloaded from https://onlinelibrary.wiley.com/doi/10.1002/cne.25589 by Cochrane Canada Provision, Wiley Online Library on [27/01/2024]. See the Terms and Conditions (https://onlinelibrary.wiley.com/terms-and-conditions) on Wiley Online Library for rules of use; OA articles are governed by the applicable Creative Commons License

Given that adult *Rai1* deletion in mice impacts metabolic functions, RAI1 may be continuously required in adult marmoset brains. While RAI1 expression profiles are similar in adult mice and marmosets, in newborn marmosets, RAI1 is detected in significantly fewer neurons, specifically excitatory but not inhibitory neurons. Comparative analyses found highly similar proportions of inhibitory neuronal subclasses and connectivity in mice, marmoset, and human cortices (Bakken et al., 2021; Kim et al., 2023). By contrast, glutamatergic neurons in humans and marmosets share more markers with each other than with mice (Bakken et al., 2021). The 30% increase of RAI1 expression observed at the transition from newborn to adult stage in marmoset, which eventually becomes similar to mice, could potentially be attributed to several factors. RAI1 is more enriched in differentiated neurons, and the primate prefrontal brains mature significantly slower than in mice (Semple et al., 2013), the lower proportion of RAI1 expression in newborn marmosets could be explained by the relatively immature developmental status of the newborn marmosets. Alternatively, retinoic acid signaling during the development of the prefrontal cortex is more similar in humans and macaques than in mice (Shibata et al., 2021), which could translate into different timing in RAI1 expression. Moreover, RAI1 expression is detected in 15% of newborn marmoset astrocytes, an observation corroborated by an RNA-sequencing study that found higher levels of *RAI1* mRNA expression in fetal rather than mature human astrocytes (Y. Zhang et al., 2014). While RAI1 loss from neurons is likely the primary driver of disease features in SMS, the contribution of astrocytic RAI1 in newborn primate brains warrants further investigation.

Structural abnormalities, such as altered neuron/astrocyte ratios (Falcone et al., 2021) and increased variability in axonal trajectories (Trutzer et al., 2019), have been identified in the upper layers of the prefrontal cortex in individuals with autism. Compared to mice, the developing prefrontal cortices of primates show an expansion of retinoic acid synthesizing enzymes and increased retinoic acid levels (Shibata et al., 2021). We found that higher RAI1 expression in patches of neurons in cortical layers II/III of newborn marmosets coexpress NEUN, consistent with a neuronal identity. In addition, 40% of these populations express NR1 or RARα. By contrast, RAI1 in newborn mice, adult mice, and adult marmosets show a broader expression pattern across cortical layers. While the mechanism that induces patchy RAI1 expression in newborn marmosets remains unclear, this pattern could imply a more restricted role for RAI1. RAI1 expression in other cortical regions and brain structures in the marmoset also awaits future investigation.

We found marmoset RAI1 expression in primate-specific cell types, including the interlaminar astrocytes that abundantly populate the superficial cortical layers. While the function of these astrocytes remains unclear, their long processes could potentially support the propagation of calcium waves (Oberheim et al., 2009). In addition, RAI1 is also expressed in primate-specific MEIS2$^+$ GABAergic neurons residing in the superficial layers of the marmoset prefrontal cortex, which in mice reside in deeper white matter (Tasic et al., 2018). Like RAI1, MEIS2 is induced by retinoic acid in primate organoids and reduced by retinoic acid receptor antagonists (Shibata et al., 2021), suggesting that both genes are part of the retinoic acid signaling pathway in newborn primate brains.

4.2 | Molecular interaction of RAI1 in the marmoset brain and human cells

Eukaryotic transcription factors commonly form protein complexes with members of the same gene family (Amoutzias et al., 2008), and such assemblies may help stabilize the protein complex to cooperatively regulate gene expression (Raab et al., 2015). In our study, RAI1 and TCF20 were highly coexpressed throughout neocortical development in marmosets and mice. Moreover, RAI1 interacted with TCF20, PHF14, and HMG20A in the developing and adult mouse and marmoset cortices, highlighting the importance of this protein complex during brain development and evolution. Importantly, we did not compare the strength of interaction between different subunits of the RAI1 protein complex because factors unrelated to the strength of protein interaction (i.e., different affinity of antibodies) could complicate the interpretation of immunoprecipitation and/or western blotting experiments. In the future, quantitative affinity purification followed by mass spectrometry studies could be performed.

The functional interaction between RAI1 and TCF20 could affect protein abundance, which may have important clinical implications. Indeed, clinical evidence shows that an increase in *RAI1* or *TCF20* dosage is detrimental to brain function. Reciprocal duplication of the SMS 17p11.2 region causes PTLS (Potocki et al., 2000), a distinct neurodevelopmental disorder that exhibits many traits mirroring those of SMS. The smallest region common to PTLS individuals carrying different 17p11.2 duplications is a 125-kb region that contains only *RAI1* (F. Zhang et al., 2010), suggesting that *RAI1* duplication underlies PTLS. Moreover, patients with neurodevelopmental disorders caused by *TCF20*-containing 22q13.2 microduplications were recently identified (Levy et al., 2021). We found that overexpressing TCF20 increases RAI1 abundance (but not vice versa), suggesting that increased RAI1 levels could contribute to disease features in patients carrying *TCF20* duplications. Interestingly, *TCF20*-KO cells show reduced RAI1 protein abundance but slightly increased *RAI1* mRNA levels, suggesting that a potential positive transcriptional feedback loop attempts to balance the mRNA levels among the protein complex subunits. A previous study reported similar findings, in which knocking down *PHF14* reduced protein levels for HMG20A but slightly higher mRNA levels (Gomez-Marin et al., 2022). A recent study showed that mouse methyl CpG binding protein 2 (MECP2, the causal gene for Rett syndrome) interacts with TCF20 and that reducing TCF20 rescues neuronal, morphological, and behavioral deficits caused by genetic *Mecp2* overexpression in mice (Zhou et al., 2022). Together with our data, these findings suggest that chromatin-interacting proteins involved in clinically distinct neurodevelopmental disorders could form protein complexes with a defined stoichiometry. Each subunit could regulate the abundance of the other subunits, and any imbalances in the composition of subunits could drive disease or modify disease progression. In the future, it would be interesting to identify protein-interacting domains between

10969861, 2024, 1, Downloaded from https://onlinelibrary.wiley.com/doi/10.1002/cne.25589 by Cochrane Canada Provision, Wiley Online Library on [27/01/2024]. See the Terms and Conditions (https://onlinelibrary.wiley.com/terms-and-conditions) on Wiley Online Library for rules of use; OA articles are governed by the applicable Creative Commons License

RAI1 and TCF20, which could provide further insights into how their protein stability is regulated.

5 | CONCLUSIONS

This study characterized the cell type-specific distributions and molecular interactions of the SMS protein RAI1 in the prefrontal cortices of common marmosets and mice. Marmoset RAI1, expressed in primate-specific cell types, shows a more restricted expression pattern than mouse RAI1 during early cortical development. At the molecular level, RAI1 forms an evolutionarily conserved protein complex with three other chromatin-binding proteins: TCF20, PHF14, and HMG20A. In human cells, TCF20 bidirectionally regulates RAI1 abundance, suggesting that imbalanced RAI1 levels could contribute to disorders caused by *TCF20* dosage imbalance.

AUTHOR CONTRIBUTIONS

Conceptualization: Ya-Ting Chang and Wei-Hsiang Huang. Biochemistry: Yu-Ju Lee and Hao-Cheng Chang. Staining, imaging, and data analysis: Ya-Ting Chang, Minza Haque, Sehrish Javed, Yu Cheng Lin, Yoobin Cho, Gabriella Chin, Asma Khamis, and Joseph Abramovitz. Data interpretation: all authors. Obtaining key resources, samples, and funding: Keith K. Murai, Reesha Raja, and Wei-Hsiang Huang. Original draft preparation: Ya-Ting Chang and Wei-Hsiang Huang, with contributions and approval from all authors.

ACKNOWLEDGMENTS

We acknowledge the funding supported by the Smith—Magenis syndrome Research Foundation and the Azrieli Centre for Autism Research.

CONFLICT OF INTEREST STATEMENT

The authors have no conflict of interest to declare.

DATA AVAILABILITY STATEMENT

The data that support the findings of this study are available from the corresponding author upon reasonable request.

ORCID

Wei-Hsiang Huang https://orcid.org/0000-0002-8411-9433

REFERENCES

Amoutzias, G. D., Robertson, D. L., Van De Peer, Y., & Oliver, S. G. (2008). Choose your partners: Dimerization in eukaryotic transcription factors. *Trends in Biochemical Sciences*, *33*(5), 220–229. https://doi.org/10.1016/j.tibs.2008.02.002

Babbs, C., Lloyd, D., Pagnamenta, A. T., Twigg, S. R. F., Green, J., Mcgowan, S. J., Mirza, G., Naples, R., Sharma, V. P., Volpi, E. V., Buckle, V. J., Wall, S. A., Knight, S. J. L., Parr, J. R., & Wilkie, A. O. M. (2014). De novo and rare inherited mutations implicate the transcriptional coregulator TCF20/SPBP in autism spectrum disorder. *Journal of Medical Genetics*, *51*(11), 737–747. https://doi.org/10.1136/jmedgenet-2014-102582

Bakken, T. E., Jorstad, N. L., Hu, Q., Lake, B. B., Tian, W., Kalmbach, B. E., Crow, M., Hodge, R. D., Krienen, F. M., Sorensen, S. A., Eggermont, J., Yao, Z., Aevermann, B. D., Aldridge, A. I., Bartlett, A., Bertagnolli, D., Casper, T., Castanon, R. G., Crichton, K., … Lein, E. S. (2021). Comparative cellular analysis of motor cortex in human, marmoset and mouse. *Nature*, *598*(7879), 111–119. https://doi.org/10.1038/s41586-021-03465-8

Bi, W., Ohyama, T., Nakamura, H., Yan, J., Visvanathan, J., Justice, M. J., & Lupski, J. R. (2005). Inactivation of Rai1 in mice recapitulates phenotypes observed in chromosome engineered mouse models for Smith—Magenis syndrome. *Human Molecular Genetics*, *14*(8), 983–995. https://doi.org/10.1093/hmg/ddi085

Bi, W., Yan, J., Shi, X., Yuva-Paylor, L. A., Antalffy, B. A., Goldman, A., Yoo, J. W., Noebels, J. L., Armstrong, D. L., Paylor, R., & Lupski, J. R. (2007). Rai1 deficiency in mice causes learning impairment and motor dysfunction, whereas Rai1 heterozygous mice display minimal behavioral phenotypes. *Human Molecular Genetics*, *16*(15), 1802–1813. https://doi.org/10.1093/hmg/ddm128

Chang, H.-C., Lee, Y.-J., Javed, S., Haque, M., Chang, Y.-T., Lin, Y. C., Oram, C., & Huang, W.-H. (2022). rAAV-CRISPRa therapy corrects Rai1 haploinsufficiency and rescues selective disease features in Smith—Magenis syndrome mice. *Journal of Biological Chemistry*, *102728*, 299. https://doi.org/10.1016/j.jbc.2022.102728

Chang, Y.-T., Kowalczyk, M., Fogerson, P. M, Lee, Y.-J., Haque, M., Adams, E. L., Wang, D. C., Denardo, L. A., Tessier-Lavigne, M., Huguenard, J. R., Luo, L., & Huang, W.-H. (2022). Loss of Rai1 enhances hippocampal excitability and epileptogenesis in mouse models of Smith—Magenis syndrome. *Proceedings of the National Academy of Sciences of the United States of America*, *119*(43), e2210122119. https://doi.org/10.1073/pnas.2210122119

Chini, M., & Hanganu-Opatz, I. L. (2021). Prefrontal cortex development in health and disease: Lessons from rodents and humans. *Trends in Neuroscience*, *44*(3), 227–240. https://doi.org/10.1016/j.tins.2020.10.017

Co, M., Barnard, R. A., Jahncke, J. N., Grindstaff, S., Fedorov, L. M., Adey, A. C., Wright, K. M., & O'roak, B. J. (2022). Shared and distinct functional effects of patient-specific Tbr1 mutations on cortical development. *Journal of Neuroscience*, *42*(37), 7166–7181. https://doi.org/10.1523/JNEUROSCI.0409-22.2022

Darvekar, S., Rekdal, C., Johansen, T., & Sjøttem, E. (2013). A phylogenetic study of SPBP and RAI1: Evolutionary conservation of chromatin binding modules. *PLoS ONE*, *8*(10), e78907. https://doi.org/10.1371/journal.pone.0078907

De Rubeis, S., He, X., Goldberg, A. P., Poultney, C. S., Samocha, K., Ercument Cicek, A., Kou, Y., Liu, L., Fromer, M., Walker, S., Singh, T., Klei, L., Kosmicki, J., Fu, S.-C., Aleksic, B., Biscaldi, M., Bolton, P. F., Brownfeld, J. M., Cai, J., … Buxbaum, J. D. (2014). Synaptic, transcriptional and chromatin genes disrupted in autism. *Nature*, *515*(7526), 209–215. https://doi.org/10.1038/nature13772

Eberl, H. C., Spruijt, C. G., Kelstrup, C. D., Vermeulen, M., & Mann, M. (2013). A map of general and specialized chromatin readers in mouse tissues generated by label-free interaction proteomics. *Molecular Cell*, *49*(2), 368–378. https://doi.org/10.1016/j.molcel.2012.10.026

Englund, C., Fink, A., Lau, C., Pham, D., Daza, R. A. M., Bulfone, A., Kowalczyk, T., & Hevner, R. F. (2005). Pax6, Tbr2, and Tbr1 are expressed sequentially by radial glia, intermediate progenitor cells, and postmitotic neurons in developing neocortex. *Journal of Neuroscience*, *25*(1), 247–251. https://doi.org/10.1523/JNEUROSCI.2899-04.2005

Falcone, C., Mevises, N.-Y., Hong, T., Dufour, B., Chen, X., Noctor, S. C., & Martínez Cerdeño, V. (2021). Neuronal and glial cell number is altered in a cortical layer-specific manner in autism. *Autism*, *25*(8), 2238–2253. https://doi.org/10.1177/13623613211014408

Falcone, C., Wolf-Ochoa, M., Amina, S., Hong, T., Vakilzadeh, G., Hopkins, W. D., Hof, P. R., Sherwood, C. C., Manger, P. R., Noctor, S. C., & Martínez-Cerdeño, V. (2019). Cortical interlaminar astrocytes across the therian mammal radiation. *Journal of Comparative Neurology*, *527*(10), 1654–1674. https://doi.org/10.1002/cne.24605

Fong, A. Y., Stornetta, R. L., Foley, C. M., & Potts, J. T. (2005). Immunohistochemical localization of GAD67-expressing neurons and processes in the rat brainstem: Subregional distribution in the nucleus tractus

10969861, 2024, 1, Downloaded from https://onlinelibrary.wiley.com/doi/10.1002/cne.25589 by Cochrane Canada Provision, Wiley Online Library on [27/01/2024]. See the Terms and Conditions (https://onlinelibrary.wiley.com/terms-and-conditions) on Wiley Online Library for rules of use; OA articles are governed by the applicable Creative Commons License

solitarius. *Journal of Comparative Neurology*, *493*(2), 274–290. https://doi.org/10.1002/cne.20758

Fragoso, Y. D., Stoney, P. N., Shearer, K. D., Sementilli, A., Nanescu, S. E., Sementilli, P., & Mccaffery, P. (2015). Expression in the human brain of retinoic acid induced 1, a protein associated with neurobehavioural disorders. *Brain Structure and Function*, *220*(2), 1195–1203. https://doi.org/10.1007/s00429-014-0712-1

Geschwind, D. H., & Rakic, P. (2013). Cortical evolution: Judge the brain by its cover. *Neuron*, *80*(3), 633–647. https://doi.org/10.1016/j.neuron.2013.10.045

Gómez-Marín, E., Posavec-Marjanović, M., Zarzuela, L., Basurto-Cayuela, L., Guerrero-Martínez, J. A., Arribas, G., Yerbes, R., Ceballos-Chávez, M., Rodríguez-Paredes, M., Tomé, M., Durán, R. V., Buschbeck, M., & Reyes, J. C. (2022). The high mobility group protein HMG20A cooperates with the histone reader PHF14 to modulate TGFbeta and Hippo pathways. *Nucleic Acids Research*, *50*(17), 9838–9857. https://doi.org/10.1093/nar/gkac766

Graham, V., Khudyakov, J., & Ellis, P., & Pevny, L. (2003). SOX2 functions to maintain neural progenitor identity. *Neuron*, *39*(5), 749–765. https://doi.org/10.1016/s0896-6273(03)00497-5

Hein, M. Y., Hubner, N. C., Poser, I., Cox, J., Nagaraj, N., Toyoda, Y., Gak, I. A., Weisswange, I., Mansfeld, J., Buchholz, F., Hyman, A. A., & Mann, M. (2015). A human interactome in three quantitative dimensions organized by stoichiometries and abundances. *Cell*, *163*(3), 712–723. https://doi.org/10.1016/j.cell.2015.09.053

Homman-Ludiye, J., Merson, T. D., & Bourne, J. A. (2012). The early postnatal nonhuman primate neocortex contains self-renewing multipotent neural progenitor cells. *PLoS ONE*, *7*(3), e34383. https://doi.org/10.1371/journal.pone.0034383

Huang, W. H. (2022). Performing single-cell clonal analysis in the mouse brain using mosaic analysis with double markers (MADM). *Methods in Molecular Biology*, *2515*, 59–74. https://doi.org/10.1007/978-1-0716-2409-8_4

Huang, W.-H., Guenthner, C. J., Xu, J., Nguyen, T., Schwarz, L. A., Wilkinson, A. W., Gozani, O., Chang, H. Y., Shamloo, M., & Luo, L. (2016). Molecular and neural functions of Rai1, the causal gene for Smith–Magenis syndrome. *Neuron*, *92*(2), 392–406. https://doi.org/10.1016/j.neuron.2016.09.019

Huang, W.-H., Tupal, S., Huang, T.-W., Ward, C. S., Neul, J. L., Klisch, T. J., Gray, P. A., & Zoghbi, H. Y. (2012). Atoh1 governs the migration of postmitotic neurons that shape respiratory effectiveness at birth and chemoresponsiveness in adulthood. *Neuron*, *75*(5), 799–809. https://doi.org/10.1016/j.neuron.2012.06.027

Huang, W.-H., Wang, D. C., Allen, W. E., Klope, M., Hu, H., Shamloo, M., & Luo, L. (2018). Early adolescent Rai1 reactivation reverses transcriptional and social interaction deficits in a mouse model of Smith–Magenis syndrome. *Proceedings of the National Academy of Sciences of the United States of America*, *115*, 10744–10749. https://doi.org/10.1073/pnas.1806796115

Imai, Y., Suzuki, Y., Matsui, T., Tohyama, M., Wanaka, A., & Takagi, T. (1995). Cloning of a retinoic acid-induced gene, GT1, in the embryonal carcinoma cell line P19: Neuron-specific expression in the mouse brain. *Brain Research Molecular Brain Research*, *31*(1–2), 1–9.

Ince-Dunn, G., Hall, B. J., Hu, S.-C., Ripley, B., Huganir, R. L., Olson, J. M., Tapscott, S. J., & Ghosh, A. (2006). Regulation of thalamocortical patterning and synaptic maturation by NeuroD2. *Neuron*, *49*(5), 683–695. https://doi.org/10.1016/j.neuron.2006.01.031

Izpisua Belmonte, J. C., Callaway, E. M., Caddick, S. J., Churchland, P., Feng, G., Homanics, G. E., Lee, K.-F., Leopold, D. A., Miller, C. T., Mitchell, J. F., Mitalipov, S., Moutri, A. R., Movshon, J. A, Okano, H., Reynolds, J. H., Ringach, D. L., Sejnowski, T. J., Silva, A. C., Strick, P. L., … Zhang, F. (2015). Brains, genes, and primates. *Neuron*, *86*(3), 617–631. https://doi.org/10.1016/j.neuron.2015.03.021

Javed, S., Chang, Y. T., Cho, Y., Lee, Y. J., Chang, H. C., Haque, M., & Huang, W. H. (2023). Smith–Magenis syndrome protein Rai1 regulates body weight homeostasis through hypothalamic Bdnf-producing neurons and neurotrophin downstream signalling. *eLife*, *12*, https://doi.org/10.7554/eLife.90333.2

Javed, S., Lee, Y.-J., Xu, J., & Huang, W.-H. (2021). Temporal dissection of Rai1 function reveals brain-derived neurotrophic factor as a potential therapeutic target for Smith–Magenis syndrome. *Human Molecular Genetics*, *31*, 275–288. https://doi.org/10.1093/hmg/ddab245

Javed, S., Selliah, T., Lee, Y.-J., & Huang, W.-H. (2020). Dosage-sensitive genes in autism spectrum disorders: From neurobiology to therapy. *Neuroscience and Biobehavioral Reviews*, *118*, 538–567. https://doi.org/10.1016/j.neubiorev.2020.08.009

Jung, S.-C., Kim, J., & Hoffman, D A. (2008). Rapid, bidirectional remodeling of synaptic NMDA receptor subunit composition by A-type K+ channel activity in hippocampal CA1 pyramidal neurons. *Neuron*, *60*(4), 657–671. https://doi.org/10.1016/j.neuron.2008.08.029

Kim, M.-H., Radaelli, C., Thomsen, E. R., Monet, D., Chartrand, T., Jorstad, N. L., Mahoney, J. T., Taormina, M. J., Long, B., Baker, K., Bakken, T. E., Campagnola, L., Casper, T., Clark, M., Dee, N., D'orazi, F., Gamlin, C., Kalmbach, B. E., Kebede, S., & Lein, E. (2023). Target cell-specific synaptic dynamics of excitatory to inhibitory neuron connections in supragranular layers of human neocortex. *eLife*, *12*, e81863, https://doi.org/10.7554/eLife.81863

Kita, Y., Nishibe, H., Wang, Y., Hashikawa, T., Kikuchi, S. S., U, M., Yoshida, A. C., Yoshida, C., Kawase, T., Ishii, S., Skibbe, H., & Shimogori, T. T. (2021). Cellular-resolution gene expression profiling in the neonatal marmoset brain reveals dynamic species- and region-specific differences. *Proceedings of the National Academy of Sciences of the United States of America*, *118*(18), https://doi.org/10.1073/pnas.2020125118

Kitagawa, M., Takebe, A., Ono, Y., Imai, T., Nakao, K., Nishikawa, S.-I., & Era, T. (2012). Phf14, a novel regulator of mesenchyme growth via platelet-derived growth factor (PDGF) receptor-alpha. *Journal of Biological Chemistry*, *287*(33), 27983–27996. https://doi.org/10.1074/jbc.M112.350074

Laje, G., Morse, R., Richter, W., Ball, J., Pao, M., & Smith, A. C. M. (2010). Autism spectrum features in Smith–Magenis syndrome. *American Journal of Medical Genetics Part C, Seminars in Medical Genetics*, *154C*(4), 456–462. https://doi.org/10.1002/ajmg.c.30275

Laursen, K. B., & Gudas, L. J. (2018). Combinatorial knockout of RAR-alpha, RARbeta, and RARgamma completely abrogates transcriptional responses to retinoic acid in murine embryonic stem cells. *Journal of Biological Chemistry*, *293*(30), 11891–11900. https://doi.org/10.1074/jbc.RA118.001951

Lee, G. H., Chhangawala, Z., Von Daake, S., Savas, J. N., Yates, J. R., Comoletti, D., & D'arcangelo, G. (2014). Reelin induces Erk1/2 signaling in cortical neurons through a non-canonical pathway. *Journal of Biological Chemistry*, *289*(29), 20307–20317. https://doi.org/10.1074/jbc.M114.576249

Lelieveld, S. H., Reijnders, M. R. F., Pfundt, R., Yntema, H. G., Kamsteeg, E.-J., De Vries, P., De Vries, B. B. A., Willemsen, M. H., Kleefstra, T., Löhner, K., Vreeburg, M., Stevens, S. J. C., Van Der Burgt, I., Bongers, E. M. H. F., Stegmann, A. P. A., Rump, P., Rinne, T., Nelen, M. R., Veltman, J. A., … Gilissen, C. (2016). Meta-analysis of 2,104 trios provides support for 10 new genes for intellectual disability. *Nature Neuroscience*, *19*(9), 1194–1196. https://doi.org/10.1038/nn.4352

Levitt, P., Cooper, M., & Rakic, P. (1981). Coexistence of neuronal and glial precursor cells in the cerebral ventricular zone of the fetal monkey: An ultrastructural immunoperoxidase analysis. *Journal of Neuroscience*, *1*(1), 27–39. https://doi.org/10.1523/JNEUROSCI.01-01-00027.1981

Levitt, P., Cooper, M. L., & Rakic, P. (1983). Early divergence and changing proportions of neuronal and glial precursor cells in the primate cerebral ventricular zone. *Developmental Biology*, *96*(2), 472–484. https://doi.org/10.1016/0012-1606(83)90184-7

Levitt, P., & Rakic, P. (1980). Immunoperoxidase localization of glial fibrillary acidic protein in radial glial cells and astrocytes of the developing rhesus monkey brain. *Journal of Comparative Neurology*, *193*(3), 815–840. https://doi.org/10.1002/cne.901930316

10969861, 2024, 1, Downloaded from https://onlinelibrary.wiley.com/doi/10.1002/cne.25589 by Cochrane Canada Provision, Wiley Online Library on [27/01/2024]. See the Terms and Conditions (https://onlinelibrary.wiley.com/terms-and-conditions) on Wiley Online Library for rules of use; OA articles are governed by the applicable Creative Commons License

Lévy, J., Cogan, G., Maruani, A., Maillard, A., Dupont, C., Drunat, S., Rachid, M., Atzori, P., Delorme, R., Jeyarajah, S., Isidor, B., Pichon, O., Moradkhani, K., Verloes, A., & Tabet, A.-C. (2021). Rare and de novo duplications containing TCF20 are associated with a neurodevelopmental disorder. *Clinical Genetics*, *101*, 364–370. https://doi.org/10.1111/cge.14099

Mcdermott, K. W. G., & Lantos, P. L. (1989). The distribution of glial fibrillary acidic protein and vimentin in postnatal marmoset (*Callithrix jacchus*) brain. *Brain Research Developmental Brain Research*, *45*(2), 169–177. https://doi.org/10.1016/0165-3806(89)90036-9

Miller, C. T., Freiwald, W. A., Leopold, D. A., Mitchell, J. F., Silva, A. C., & Wang, X. (2016). Marmosets: A neuroscientific model of human social behavior. *Neuron*, *90*(2), 219–233. https://doi.org/10.1016/j.neuron.2016.03.018

Mitchell, J. F., & Leopold, D. A. (2015). The marmoset monkey as a model for visual neuroscience. *Neuroscience Research*, *93*, 20–46. https://doi.org/10.1016/j.neures.2015.01.008

Mullen, R. J., Buck, C. R., & Smith, A. M. (1992). NeuN, a neuronal specific nuclear protein in vertebrates. *Development (Cambridge, England)*, *116*(1), 201–211. https://doi.org/10.1242/dev.116.1.201

Muñoz, Y., Cuevas-Pacheco, F., Quesseveur, G., & Murai, K. K. (2021). Light microscopic and heterogeneity analysis of astrocytes in the common marmoset brain. *Journal of Neuroscience Research*, *99*, 3121–3147. https://doi.org/10.1002/jnr.24967

Namba, T., Mochizuki, H., Onodera, M., Mizuno, Y., Namiki, H., & Seki, T. (2005). The fate of neural progenitor cells expressing astrocytic and radial glial markers in the postnatal rat dentate gyrus. *European Journal of Neuroscience*, *22*(8), 1928–1941. https://doi.org/10.1111/j.1460-9568.2005.04396.x

Oberheim, N. A., Takano, T., Han, X., He, W., Lin, J. H. C., Wang, F., Xu, Q., Wyatt, J. D., Pilcher, W., Ojemann, J. G., Ransom, B. R., Goldman, S. A., & Nedergaard, M. (2009). Uniquely hominid features of adult human astrocytes. *Journal of Neuroscience*, *29*(10), 3276–3287. https://doi.org/10.1523/JNEUROSCI.4707-08.2009

Ogawa, M., Miyata, T., Nakajimat, K., Yagyu, K., Seike, M., Ikenaka, K., Yamamoto, H., & Mikoshibat, K. (1995). The reeler gene-associated antigen on Cajal—Retzius neurons is a crucial molecule for laminar organization of cortical neurons. *Neuron*, *14*(5), 899–912. https://doi.org/10.1016/0896-6273(95)90329-1

Potocki, L., Chen, K.-S., Park, S.-S., Osterholm, D. E., Withers, M. A., Kimonis, V., Summers, A. M., Meschino, W. S., Anyane-Yeboa, K., Kashork, C. D., Shaffer, L. G., & Lupski, J. R. (2000). Molecular mechanism for duplication 17p11.2—The homologous recombination reciprocal of the Smith–Magenis microdeletion. *Nature Genetics*, *24*(1), 84–87. https://doi.org/10.1038/71743

Raab, J. R., Resnick, S., & Magnuson, T. (2015). Genome-wide transcriptional regulation mediated by biochemically distinct SWI/SNF complexes. *PLoS Genetics*, *11*(12), e1005748. https://doi.org/10.1371/journal.pgen.1005748

Rao, N., Abad, C., Perez, I., Srivastava, A., Young, J., & Walz, K. (2017). Rai1 haploinsufficiency is associated with social abnormalities in mice. *Biology (Basel)*, *6*(2), 25. https://doi.org/10.3390/biology6020025

Rash, B. G., Duque, A., Morozov, Y. M., Arellano, J. I., Micali, N., & Rakic, P. (2019). Gliogenesis in the outer subventricular zone promotes enlargement and gyrification of the primate cerebrum. *Proceedings of the National Academy of Sciences of the United States of America*, *116*(14), 7089–7094. https://doi.org/10.1073/pnas.1822169116

Schäfgen, J., Cremer, K., Becker, J., Wieland, T., Zink, A. M., Kim, S., Windheuser, I. C., Kreiß, M., Aretz, S., Strom, T. M., Wieczorek, D., & Engels, H. (2016). De novo nonsense and frameshift variants of TCF20 in individuals with intellectual disability and postnatal overgrowth. *European Journal of Human Genetics*, *24*(12), 1739–1745. https://doi.org/10.1038/ejhg.2016.90

Schmitz, M. T., Sandoval, K., Chen, C. P., Mostajo-Radji, M. A., Seeley, W. W., Nowakowski, T. J., Ye, C. J., Paredes, M. F., & Pollen, A. A. (2022). The development and evolution of inhibitory neurons in primate cerebrum. *Nature*, *603*(7903), 871–877. https://doi.org/10.1038/s41586-022-04510-w

Semple, B. D., Blomgren, K., Gimlin, K., Ferriero, D. M., & Noble-Haeusslein, L. J. (2013). Brain development in rodents and humans: Identifying benchmarks of maturation and vulnerability to injury across species. *Progress in Neurobiology*, *106–107*, 1–16. https://doi.org/10.1016/j.pneurobio.2013.04.001

She, K., Ferreira, J. S., Carvalho, A. L., & Craig, A. M. (2012). Glutamate binding to the GluN2B subunit controls surface trafficking of N-methyl-D-aspartate (NMDA) receptors. *Journal of Biological Chemistry*, *287*(33), 27432–27445. https://doi.org/10.1074/jbc.M112.345108

Shibata, M., Pattabiraman, K., Lorente-Galdos, B., Andrijevic, D., Kim, S.-K., Kaur, N., Muchnik, S. K., Xing, X., Santpere, G., Sousa, A. M. M., & Sestan, N. (2021). Regulation of prefrontal patterning and connectivity by retinoic acid. *Nature*, *598*(7881), 483–488. https://doi.org/10.1038/s41586-021-03953-x

Slager, R. E., Newton, T. L., Vlangos, C. N., Finucane, B., & Elsea, S. H. (2003). Mutations in RAI1 associated with Smith—Magenis syndrome. *Nature Genetics*, *33*(4), 466–468. https://doi.org/10.1038/ng1126

Smith, A. C., Dykens, E., & Greenberg, F. (1998). Behavioral phenotype of Smith—Magenis syndrome (del 17p11.2). *American Journal of Medical Genetics*, *81*(2), 179–185. https://doi.org/10.1002/(sici)1096-8628(19980328)81:2⟨179::aid-ajmg10⟩3.0.co;2-e

Taggart, J. C., Zauber, H., Selbach, M., Li, G.-W., & Mcshane, E. (2020). Keeping the proportions of protein complex components in check. *Cell Systems*, *10*(2), 125–132. https://doi.org/10.1016/j.cels.2020.01.004

Tanga, F. Y., Raghavendra, V., Nutile-Mcmenemy, N., Marks, A., & Deleo, J. A. (2006). Role of astrocytic S100beta in behavioral hypersensitivity in rodent models of neuropathic pain. *Neuroscience*, *140*(3), 1003–1010. https://doi.org/10.1016/j.neuroscience.2006.02.070

Tasic, B., Yao, Z., Graybuck, L. T., Smith, K. A., Nguyen, T. N., Bertagnolli, D., Goldy, J., Garren, E., Economo, M. N., Viswanathan, S., Penn, O., Bakken, T., Menon, V., Miller, J., Fong, O., Hirokawa, K E., Lathia, K., Rimorin, C., Tieu, M., … Zeng, H. (2018). Shared and distinct transcriptomic cell types across neocortical areas. *Nature*, *563*(7729), 72–78. https://doi.org/10.1038/s41586-018-0654-5

Torti, E., Keren, B., Palmer, E. E., Zhu, Z., Afenjar, A., Anderson, I. J., Andrews, M. V., Atkinson, C., Au, M., Berry, S. A., Bowling, K. M., Boyle, J., Buratti, J., Cathey, S. S., Charles, P., Cogne, B., Courtin, T., Escobar, L. F., Finley, S. L., … Juusola, J. (2019). Variants in TCF20 in neurodevelopmental disability: Description of 27 new patients and review of literature. *Genetics in Medicine*, *21*(9), 2036–2042. https://doi.org/10.1038/s41436-019-0454-9

Trost, B., Thiruvahindrapuram, B., Chan, A. J. S., Engchuan, W., Higginbotham, E. J., Howe, J. L., Loureiro, L. O., Reuter, M. S., Roshandel, D., Whitney, J., Zarrei, M., Bookman, M., Somerville, C., Shaath, R., Abdi, M., Aliyev, E., Patel, R. V., Nalpathamkalam, T., Pellecchia, G., … Scherer, S. W. (2022). Genomic architecture of autism from comprehensive whole-genome sequence annotation. *Cell*, *185*(23), 4409–4427. https://doi.org/10.1016/j.cell.2022.10.009

Trutzer, I. M., García-Cabezas, M. Á., & Zikopoulos, B. (2019). Postnatal development and maturation of layer 1 in the lateral prefrontal cortex and its disruption in autism. *Acta Neuropathologica Communications*, *7*(1), 40. https://doi.org/10.1186/s40478-019-0684-8

Upadia, J., Gonzales, P. R., Atkinson, T. P, Schroeder, H. W., Robin, N. H., Rudy, N. L., & Mikhail, F. M. (2018). A previously unrecognized 22q13.2 microdeletion syndrome that encompasses TCF20 and TNFRSF13C. *American Journal of Medical Genetics. Part A*, *176*(12), 2791–2797. https://doi.org/10.1002/ajmg.a.40492

Vetrini, F., Mckee, S., Rosenfeld, J. A., Suri, M., Lewis, A. M., Nugent, K. M., Roeder, E., Littlejohn, R. O., Holder, S., Zhu, W., Alaimo, J. T., Graham, B., Harris, J. M., Gibson, J. B., Pastore, M., Mcbride, K. L., Komara, M., Al-Gazali, L., Al Shamsi, A., … Liu, P. (2019). De novo and inherited TCF20 pathogenic variants are associated with intellectual disability, dysmorphic features, hypotonia, and neurological impairments with similarities

10969861, 2024, 1, Downloaded from https://onlinelibrary.wiley.com/doi/10.1002/cne.25589 by Cochrane Canada Provision, Wiley Online Library on [27/01/2024]. See the Terms and Conditions (https://onlinelibrary.wiley.com/terms-and-conditions) on Wiley Online Library for rules of use; OA articles are governed by the applicable Creative Commons License

to Smith–Magenis syndrome. *Genome Medicine*, *11*(1), 12. https://doi.org/10.1186/s13073-019-0623-0

Zhang, C., Zhu, H., Ni, Z., Xin, Q., Zhou, T., Wu, R., Gao, G., Gao, Z., Ma, H., Li, H., He, M., Zhang, J., Cheng, H., & Hu, H. (2022). Dynamics of a disinhibitory prefrontal microcircuit in controlling social competition. *Neuron*, *110*(3), 516–531. https://doi.org/10.1016/j.neuron.2021.10.034

Zhang, F., Potocki, L., Sampson, J. B., Liu, P., Sanchez-Valle, A., Robbins-Furman, P., Navarro, A. D., Wheeler, P. G., Spence, J. E, Brasington, C. K., Withers, M. A., & Lupski, J. R. (2010). Identification of uncommon recurrent Potocki–Lupski syndrome-associated duplications and the distribution of rearrangement types and mechanisms in PTLS. *American Journal of Human Genetics*, *86*(3), 462–470. https://doi.org/10.1016/j.ajhg.2010.02.001

Zhang, Y., Chen, K., Sloan, S. A., Bennett, M. L., Scholze, A. R., O'keeffe, S., Phatnani, H. P., Guarnieri, P., Caneda, C., Ruderisch, N., Deng, S., Liddelow, S. A., Zhang, C., Daneman, R., Maniatis, T., Barres, B. A., & Wu, J. Q. (2014). An RNA-sequencing transcriptome and splicing database of glia, neurons, and vascular cells of the cerebral cortex. *Journal of Neuroscience*, *34*(36), 11929–11947. https://doi.org/10.1523/JNEUROSCI.1860-14.2014

Zhao, S., Chai, X., Bock, H. H., Brunne, B., Förster, E., & Frotscher, M. (2006). Rescue of the reeler phenotype in the dentate gyrus by wild-type coculture is mediated by lipoprotein receptors for Reelin and Disabled 1. *Journal of Comparative Neurology*, *495*(1), 1–9. https://doi.org/10.1002/cne.20846

Zhou, J., Hamdan, H., Yalamanchili, H. K., Pang, K., Pohodich, A. E., Lopez, J., Shao, Y., Oses-Prieto, J. A., Li, L., Kim, W., Durham, M. A., Bajikar, S. S., Palmer, D. J., Ng, P., Thompson, M. L., Bebin, E. M, Müller, A. J., Kuechler, A., Kampmeier, A., … Zoghbi, H. Y. (2022). Disruption of MeCP2-TCF20 complex underlies distinct neurodevelopmental disorders. *Proceedings of the National Academy of Sciences of the United States of America*, *119*(4), https://doi.org/10.1073/pnas.2119078119

SUPPORTING INFORMATION

Additional supporting information can be found online in the Supporting Information section at the end of this article.

How to cite this article: Chang, Y.-T, Lee, Y.-J., Haque, M., Chang, H.-C., Javed, S., Lin, Y. C, Cho, Y., Abramovitz, J., Chin, G., Khamis, A., Raja, R., Murai, K. K., & Huang, W.-H. (2024). Comparative analyses of the Smith–Magenis syndrome protein RAI1 in mice and common marmoset monkeys. *Journal of Comparative Neurology*, *532*, e25589. https://doi.org/10.1002/cne.25589

10969861, 2024, 1, Downloaded from https://onlinelibrary.wiley.com/doi/10.1002/cne.25589 by Cochrane Canada Provision, Wiley Online Library on [27/01/2024]. See the Terms and Conditions (https://onlinelibrary.wiley.com/terms-and-conditions) on Wiley Online Library for rules of use; OA articles are governed by the applicable Creative Commons License